Measuring plume-related exhumation of the British Isles in Early Cenozoic times

Nathan Cogné[1]*, Daniel Doepke[1], David Chew[1], Finlay M. Stuart[2] and Chris Mark[1]

[1]Department of Geology, Trinity College Dublin, College Green, Dublin 2, Ireland.

[2]SUERC, Rankine Avenue, Scottish Enterprise Technology Park, East Kilbride G75 0QF, United Kingdom.

* Corresponding Author: cognen@tcd.ie

Abstract

Mantle plumes have been proposed to exert a first-order control on the morphology of Earth's surface. However, there is little consensus on the lifespan of the convectively supported topography. Here, we focus on the Cenozoic uplift and exhumation history of the British Isles. While uplift in the absence of major regional tectonic activity has long been documented, the causative mechanism is highly controversial, and direct exhumation estimates are hindered by the near-complete absence of onshore post-Cretaceous sediments (outside Northern Ireland) and the truncated stratigraphic record of many offshore basins. Two main hypotheses have been developed by previous studies: epeirogenic exhumation driven by the proto-Iceland plume, or multiple phases of Cenozoic compression driven by far-field stresses. Here, we present a new thermochronological dataset comprising 43 apatite fission track (AFT) and 102 (U-Th-Sm)/He (AHe) dates from the onshore British Isles. Inverse modelling of vertical sample profiles allows us to define well-constrained regional cooling histories. Crucially, during the Paleocene, the thermal history models show that a rapid exhumation pulse (1-2.5 km) occurred, focussed on the Irish Sea.

Exhumation is greatest in the north of the Irish Sea region, and decreases in intensity to the south and west. The spatial pattern of Paleocene exhumation is in agreement with the extent of magmatic underplating inferred from geophysical studies, and the timing of uplift and exhumation is synchronous with emplacement of the plume-related British and Irish Paleogene Igneous Province (BIPIP). Prior to the Paleocene exhumation pulse, the Mesozoic onshore exhumation pulse is mainly linked to the uplift and erosion of the hinterland during the complex and long-lived rifting history of the neighbouring offshore basins. The extent of Neogene exhumation is difficult to constrain due to the poor sensitivity of the AHe and AFT systems at low temperatures. We conclude that the Cenozoic topographic evolution of the British Isles is the result of plume-driven uplift and exhumation, with inversion under compressive stress playing a secondary role.

Keywords: British Isles; exhumation; low temperature thermochronology; Early Cenozoic; Iceland Plume

1. Introduction

It has long been proposed that mantle processes exert a first-order control on the Earth's topography (e.g. Cox, 1989). The topographic response to mantle upwelling can be either transient, with dynamically supported uplift and exhumation driven by mantle upwelling, or permanent, if driven by magmatic underplating (White and McKenzie, 1989). While the temperature anomaly associated with mantle plumes can propagate through the sub-lithospheric mantle over 1,000 km radially (White and McKenzie, 1989), the magnitude of induced uplift and exhumation can be

hard to discriminate from intra-plate exhumation caused by horizontally-transmitted far-field tectonic stresses (Burov and Cloetingh, 2009, Braun, 2010).

In this contribution we focus on the controversial question of whether a long-recognised phase of post-Cretaceous exhumation in the British Isles was generated by upwelling mantle of the proto-Iceland plume (Davis et al., 2012), or by far-field tectonic stresses transmitted from the Alpine collision (Hillis et al., 2008). The Iceland plume is generally regarded as the source for Cenozoic anomalous magmatic activity and dynamic support throughout Greenland and the North Atlantic basin (e.g., Jones and White, 2003). This includes the British Paleogene Igneous Province (BIPIP), emplaced between ca. 63-58 Ma (Ganerød et al., 2010), which shows a clear proto-Iceland plume geochemical signature (Stuart et al., 2000). Thus the Irish Sea area encompassed the zone of influence of the plume in the early Paleogene times. At this time, important (i.e. kilometric scale) exhumation of the region took place (e.g., Rowley and White, 1998). However, as localised, poorly-dated inversion structures caused by compressive stresses are also reported in the British Isles throughout the Cenozoic era (e.g., Ziegler et al., 1995), the driving mechanism of the post-Cretaceous exhumation of the British Isles remains controversial (e.g., Hillis et al., 2008).

2. Geological Context and Study Approach

The post-Variscan evolution of Britain and Ireland and much of north-western Europe is characterized by orogenic collapse and prolonged extension, primarily in the Mesozoic times, which formed the basins of the Atlantic margin and the Irish and North Seas. Repeated episodes of exhumation are superimposed on these tectonic

events, recorded by erosional unconformities in the Irish Sea basins, together with onshore and offshore AFT ages, vitrinite reflectance, sediment compaction studies and subsidence analyses (Rowley and White, 1998; Holford et al., 2005; Hillis et al., 2008). The Mesozoic exhumation episodes are variously attributed to either uplift induced by the dynamic support provided by mantle convection (Jones et al., 2012, and references therein) or to transmitted stresses from pre-existing, or incipient plate boundaries (Holford et al., 2005).

Determining the Cenozoic geological evolution of the British Isles is hindered by the paucity of Cenozoic onshore outcrops outside of Northern Ireland and the truncated stratigraphic record in many of the more accessible inboard basins. There is no consensus on the extent, magnitude, or timing of the Cenozoic event(s) (e.g. Hillis et al., 2008; Davis et al., 2012), for which two competing hypotheses have been proposed: (i) an epeirogenic mechanism linked to the proto-Iceland plume, either by Early Paleogene plume-related magmatic underplating or dynamic support (e.g. Brodie and White, 1994; Rowley and White, 1998; Jones et al., 2002) or (ii) basin inversion under compressive stress from the opening of the North Atlantic and the Alpine orogeny (e.g. Ziegler et al., 1995; Holford et al., 2005; Hillis et al., 2008).

The greatest magnitude of Cenozoic exhumation is generally reported around the Irish Sea region (Lewis et al., 1992; Al-Kindi et al., 2003), which is the focus of this study. The Irish Sea (including its southern extensions, the St George's Channel and Bristol Channel), and the Celtic Sea to the south, comprise a series of fully-filled, partially-inverted post-Variscan basins with little bathymetric expression, hosting late Carboniferous to Cenozoic sedimentary units (Rowley and White, 1998; Naylor and Shannon, 2009). Topographically, the Irish Sea is today merely a shallow (up to ca. 120 m) marine embayment, which is likely related to ice-stream excavation and

glacial palaeo-loading. The Celtic Sea basin preserves Jurassic and Cretaceous successions, and in common with the North Sea and the Western Irish offshore basins, these Mesozoic successions yield evidence for at least two episodes of exhumation during Mid-Jurassic times and at the Jurassic / Cretaceous boundary (Jones et al., 2012). However these episodes cannot be observed directly in the north part of the Irish Sea basin system, as Mesozoic sedimentary rocks of post-Early Jurassic age are generally absent (Naylor and Shannon, 2009), demonstrating that a significant portion of the post-rift sequence is missing. Cenozoic sedimentary rocks in the Irish Sea are only preserved locally in the St George's Channel Basin, where > 1km of Eocene-Oligocene sediments are preserved (Williams et al., 2005), and in the Cardigan Bay Basin where a ca. 600 m thick sequence of Oligocene-Miocene succession is reported (Naylor and Shannon, 2009). Cenozoic exhumation, including partial basin exhumation, has therefore long been recognised in the Irish Sea region (e.g. Kamerling, 1979).

Late Cretaceous chalk is present in the Ulster Basin in NE Ireland (Figure S1), and underwent subaerial erosion prior to burial by the Paleocene Antrim Plateau Basalts (Simms, 2009). Similar evidence for uplift and erosion in the Paleocene is present in Mull and Morven in western Scotland (Figure S1). Outside of these regions, the lack of onshore post-Variscan sedimentary rocks around the Irish Sea basin system makes it difficult to infer the Mesozoic to Cenozoic geological evolution. Several previous studies have utilised the apatite fission-track (AFT) low-temperature thermochronometer (Lewis et al., 1992; Green et al., 1997; Green et al., 2000; Allen at al., 2002; Green, 2002; Holford et al., 2005) to quantify and date exhumation. However, the thermal sensitivity of the AFT system alone (120-60°C; Donelick et al., 2005) is not well suited to detect cooling from shallow crustal depths of 1 – 3 km.

Green et al. (2000) argued that Ireland has suffered repeated cycles of exhumation and reburial during the Mid-Jurassic, Early Cretaceous, Early Cenozoic and a final exhumation event during Neogene times. Allen et al. (2002) preferred a more continuous exhumation history with reburial restricted to the Late Cretaceous period followed by rapid exhumation during the Cenozoic times. Using a combination of apatite (U-Th)/He and AFT dating of vertical profiles from the western Irish onshore, Cogné et al. (2014) showed that the Mesozoic exhumation history of western Ireland was closely linked to the rifting history of the Atlantic margin basins to the west. The Cenozoic history was poorly constrained, and an Early Cenozoic exhumation pulse was not detected. AFT studies from the eastern side of the Irish Sea suggest that exhumation of 2 to 3 km occurred during the Early Cenozoic epoch in NE England (Lewis et al., 1992, Green et al., 1997, Green, 2002). This did not, apparently, extend to North Wales (Holford et al., 2005), where the only reported exhumation event occurred during the Triassic – Early Jurassic times. On a regional scale, however, the outcrop pattern of post-Triassic sedimentary rocks in Britain strongly suggests southeast-directed tilting during the Early Cenozoic (Cope, 1994), while the provenance of heavy mineral assemblages in the Paleogene sands of the Hampshire Basin suggests a source in Scotland (Morton, 1982), implying that that NW Britain was being uplifted at that time.

The timing of onshore and offshore exhumation in the Irish Sea region thus remains controversial, and the relative importance of Jurassic to Early Cretaceous syn-rift versus Early Cenozoic to Neogene post-rift exhumation events remains unclear (Rowley and White, 1998; Holford et al., 2005, Hillis et al., 2008, Davis et al., 2012). In this study, we combine the AFT system with the apatite (U-Th-Sm)/He (AHe) technique, which is sensitive to temperatures between 110°C and 40°C

(Shuster and Farley, 2009) to yield better-constrained thermal history models on the onshore part of Britain and Ireland. Crucially, we also employ a pseudo-vertical profile sampling approach (i.e. summit-to-valley transects) that significantly strengthens the models as they have to respect data constraints from multiple samples, which results in significantly smaller uncertainties than modelling samples independently (Gallagher et al., 2005). Combining the AFT and AHe systems with inverse modelling of vertical sample profiles therefore allows us to define the cooling history of the Irish Sea region by constraining small magnitude exhumation phases (ca. 1 km), which conventional approaches (such as modelling of fission-track data from individual samples) could fail to detect.

3. Thermochronology

3.1 Sampling strategy

We favoured a pseudo-vertical profile sampling approach (i.e., summit-to-valley sample transects) wherever permitted by lithology and topography. However in some areas (mainly northeast Ireland and the Southern Uplands in Scotland) we employed single samples that were modelled individually. In total seven vertical profiles were sampled; four in Ireland, two in Wales and one from the Paleocene Isle of Arran Northern Granite (Fig. 1). Three samples were collected from the Isle of Man, including two from the same profile but with a small vertical offset. Importantly, one sample from northeast Ireland was taken from a borehole with a present-day depth of 1702 m below surface. In total, we obtained 43 AFT ages and 102 (U-Th-Sm)/He individual ages.

176 *3.2 Fission track analyses*

177 The detailed apatite fission track methodology is described in the
178 supplementary material. All samples were prepared and analysed in Trinity College
179 Dublin (TCD) using the etching protocol of Donelick et al. (2005). Uranium
180 concentration measurements for fission track dating were undertaken by LA-ICPMS
181 at TCD following the protocols described in Donelick et al. (2005) and Cogné et al.
182 (2014). Apatite U-Pb age data were also obtained from the same LA-ICPMS spot
183 ablations with data reduction procedures following Chew et al. (2014). U-Pb data
184 were only acquired for use as high temperature constraints for the modelling
185 procedure (see thermal history modelling methodology section below) and are not
186 presented here as they do not impact on the interpretations of the Mesozoic -
187 Cenozoic thermal histories.

188

189 *3.3 (U-Th-Sm)/He*

190 A full description of the (U-Th-Sm)/He methodology is provided in the
191 supplementary material. All apatite grains were picked in TCD, and all (U-Th-Sm)/He
192 measurements were carried out at the Scottish Universities Environmental Research
193 Centre (SUERC). All procedures are described in detail in Foeken et al. (2006). The
194 minimum uncertainty on the calculated ages of the apatite unknowns is fixed at 8%
195 based on repeated (U-Th-Sm)/He measurements of the Durango apatite standard.

196

197 **4. Results**

198

199 For surface samples (excluding the Paleocene Isle of Arran Northern Granite),
200 the AFT ages range from 60.4 ± 4.0 Ma to 299.2 ± 27.6 Ma (all AFT age

uncertainties in this study are reported at the 2σ level; Table 1; Fig. 2). The mean track length (MTL) ranges from 12.5 ± 0.25 μm to 13.9 ± 0.22 μm (1 SE) with standard deviations between 1.06 μm and 1.82 μm. The kinetic parameter (D_{par}; e.g., Donelick et al., 2005) is relatively small for all samples, ranging from 1.52 to 2.1 μm, similar to Durango apatite (mean D_{par} measured for the same etching protocol is 1.66 μm). The Ire-10 and Isle of Arran samples exhibit Early Cenozoic AFT ages, which are explained by the present-day temperature of the Ire-10 sample (collected 1702m below the surface), and the Paleocene emplacement age of the Isle of Arran Northern Granite. Excluding these samples, only two samples yield Late Cretaceous/Early Cenozoic AFT ages, and they are located on the Isle of Man (IoM-3) and the Southern Uplands (Sct-1). The rest of the samples show a large spread in AFT age from the Permian to the Early Cretaceous.

The F_T-corrected AHe ages of the surface samples range from 42.7 ± 3.4 Ma to 248.6 ± 19.9 Ma (all AHe age uncertainties are reported at the 1σ level; Table 2, Fig. 2). The borehole sample (Ire-10) yielded younger AHe ages due to its higher present-day temperature. In contrast to the AFT ages, many samples from around the Irish Sea exhibit Late Cretaceous/Early Cenozoic AHe cooling ages (Fig. 2). Some grains yield older F_T-corrected ages than their corresponding AFT age. The amount of α-recoil damage within the apatite crystal lattice has a strong influence on the effective closure temperature of the AHe system (e.g. Green et al. 2006, Shuster and Farley 2009), which can be approximated by the effective uranium (eU) factor where eU = [U] + 0.24 [Th] (Green et al., 2006). In our dataset, the eU factor and AHe age are only weakly correlated, but most of the He aliquots that yield older AHe ages than the corresponding AFT age exhibit relatively high eU values. For these

aliquots, the effective closure temperature for the AHe system could be higher than that of the AFT system which would thus explain the old AHe ages.

5. Thermal history modelling methodology

Inverse modelling of the AHe and AFT (track length and age) data was undertaken to extract thermal history information. We used the QTQt software of Gallagher (2012), which employs a Bayesian trans-dimensional Markov Chain Monte Carlo (MCMC) approach. The modelling procedure is described in detail in Gallagher (2012).

In this study, a general time-temperature box with a temperature range of 75 ± 75°C (which spans the upper-temperature sensitivity limit of the AFT system to the present-day surface temperature) and a time range (which spans from the present day back to a sample-specific starting point) is used as the parameter space. A series of discrete time-temperature points are sampled within this time-temperature space to construct a continuous thermal history, and the data likelihood is then calculated for that model. To model the fission track data, we used the individual track count data, the length and angle to the c-axis of confined tracks, the annealing model of Ketcham et al. (2007) and the likelihood function of Gallagher (1995). The measured AHe ages were modelled using a spherical diffusion formulation which simulates both α-ejection and diffusion during the evolution of the thermal history (Meesters and Dunai, 2002), combined with the radiation damage model of Flowers et al. (2009). Additionally, the eU parameter is allowed to vary by up to 25% to take into account uncertainties on the apatite grain-size measurements, deviation from an ideal euhedral shape, and possible minor zonation of parent nuclides.

The present-day surface temperature for the sample is dependent on the sample elevation, and is typically set at between 15 ± 5°C and 5 ± 5°C. For the vertical profiles, the present-day offset between the top and bottom sample is set at 8 ± 3°C/km to take into account the change of surface temperature with elevation. We also employed independent geological evidence for the starting time-temperate constraint for each model, such as either the depositional age of the sample, the timing of the last regional metamorphic event experienced by the sample, or the sample U-Pb apatite age as determined by LA-ICPMS. The number of iterations depends on the stability of the likelihood chain (see Gallagher, 2012 for details), but was always set at a minimum of 200,000 iterations for single samples and at 400,000 iterations for vertical profiles.

Expected models are presented. They are essentially a weighted-mean model, while credible intervals (the Bayesian equivalent of confidence intervals) were calculated using the ensemble of thermal history solutions. These credible intervals represent the range of the model parameters contained in the posterior distribution at the specified level of probability (i.e., 95%).

In addition to the inverse modelling, forward modelling has been undertaken for some samples to test whether we could extract more information than provided by the inverse models. All the predictions (i.e., modelled versus observed ages or track-length distributions) associated with the presented models are provided in the supplementary material.

6. Synthesis of the thermal history models

A detailed description of the thermal history models including the high-temperature constraints, the geometry of the cooling/reheating path and the timing of cooling/reheating pulses is provided in the Supplementary Materials, and forms the basis of the synthesis of the thermal history models described below.

6.1 Late Paleozoic and Mesozoic thermal history

The models indicate that all the profiles in Palaeozoic rocks (i.e., excluding the Paleocene Isle of Arran Northern Granite) underwent rapid cooling following the last significant regional high-temperature event (the Variscan or Caledonian orogenies) and had entered the apatite PAZ by the beginning of the Mesozoic era. The thermal histories modelled from the single samples have larger uncertainties and do not contradict the cooling histories from the profiles. All the Palaeozoic samples had entered the apatite PAZ by the beginning of Mesozoic times.

A discrete pulse of Mesozoic cooling is evident in almost all profiles, while the thermal histories for individual samples can still accommodate such a cooling phase although it is poorly constrained due to the larger confidence intervals on these models. In Wales, the first recognised period of cooling occurred in North Snowdonia (Fig. 3a) and Pembrokeshire (Fig. 3b) during Permo-Triassic times. In North Wales this is coeval with an important rifting episode in the East Irish Sea Basin and in the Cheshire Basin (Rowley and White, 1998). In Anglesey, the Mesozoic cooling episode occurred later during Early to Middle Jurassic times (Fig. 3b), which is contemporaneous with an important phase of rifting and clastic sediment deposition in the Cardigan Bay Basin (Naylor and Shannon 2009). This history is similar to that depicted by Holford et al. (2005) for NW Wales. In South Wales, the first cooling episode recognised in Pembrokeshire is contemporaneous with the Permo-Triassic

299 opening of the Bristol Channel to the south (Kamerling, 1979), and with the opening
300 of the St George's Channel Basin to the north during Triassic times (Welch and
301 Turner, 2000). Further east, the large end-Triassic cooling pulse in the Brecon
302 Beacons (Fig. 3c) is synchronous with the onset of the main phase of deposition in
303 the East Bristol Channel Basin (Kamerling, 1979).

304 In southern Ireland, the Galtee Mountains (Fig. 4a) and Mount Leinster (Fig.
305 4b) profiles show an important phase of cooling during the Early Jurassic period,
306 similar to the episode recognised by Green et al. (2000). This is compatible with a
307 thick Triassic to Early Jurassic sedimentary sequence in the North Celtic Sea Basin
308 to the south, and with a major rifting episode in the Central Irish Sea Basin to the
309 southeast (Naylor and Shannon 2009). The Slieve Bloom profile in central Ireland
310 (Fig. 4c) shows a rather limited phase of Mesozoic cooling compared to all other
311 profiles examined in this study, with a minor acceleration in cooling rate around the
312 Jurassic-Cretaceous boundary at ca. 145 Ma. This is coeval with the cooling episode
313 recognised by Cogné et al. (2014) in vertical profiles from the western Ireland
314 onshore but is of smaller magnitude. The Lugnaquilla profile (Fig. 4d) records a pulse
315 of cooling towards the end of the Early Cretaceous period at 110 Ma, similar to the
316 cooling pulse detected in the forward model from the Isle of Man profile (Fig. 5a).
317 This Early Cretaceous cooling episode has been widely detected in Central and East
318 Irish Sea basins (Holford et al., 2005) as well as onshore Ireland (Green et al., 2000).

319 The timing and spatial distribution of Mesozoic cooling in Ireland and western
320 Britain is thus complex and lasted over 150 Ma. It has been argued that two
321 Mesozoic exhumation episodes occurred in the vicinity of the British Isles during Mid-
322 Jurassic (ca. 175 Ma) and Early Cretaceous (ca. 140 Ma) times, due to the presence
323 of large swells that induced the development of dynamic topography over a large

region (e.g. Jones et al., 2012). However, our data seems to indicate that the Mesozoic cooling episodes recorded by our samples have a more local spatial extent, as they occurred at different times during the Mesozoic over a distance of only few tens to one hundred kilometres. While a convectively-supported exhumation mechanism can explain a component of the Mesozoic exhumation, localised uplift induced by the flexural response to extension over 50 to 100 km length scales, would explain how each profile records a localised and different cooling history. Therefore we link the late Permian to Jurassic cooling episodes primarily to the complex rifting history of the basins and sub-basins in the Irish Sea and Celtic Sea. Each region appears to have experienced cooling that is synchronous with the deposition of syn-rift sediments in the closest offshore basins. The Slieve Bloom profile is the furthest from the coast and is the only profile that does not show an important cooling episode during the Mesozoic era, showing that the flexural response diminishes rapidly away from the offshore basins, in accordance with the low elastic thickness of the British Isles' lithosphere (Tiley et al., 2003). Thus cooling is likely to be mainly linked to rift-related uplift and subsequent erosion of the hinterland during the extensional episodes that formed the different sub-basins of the Irish Sea basin system. However the Bayesian modelling approach employed in this study tends to favour simpler solutions (see Gallagher, 2012), and thus might not be able to discriminate between discrete episodes of cooling that are close together in time. Assuming a palaeogeothermal gradient of 25°C/km similar to the present day (Goodman et al., 2004, Downing and Gray, 1986), the total amount of Mesozoic rift-related exhumation ranged between 1.5 and 3 km in the studied profiles.

While the onshore Mesozoic exhumation pulse can be linked to rifting in the closest offshore basins for most of the profiles, the onshore Early Cretaceous

exhumation phase seen in the Lugnaquilla and Isle of Man profiles does not have a corresponding rifting episode in the Irish Sea basin system. On the contrary, low-temperature thermochronology data for the East Irish Sea Basin and Central Irish Sea Basin suggest that the Early Cretaceous was associated with a phase of exhumation (Holford et al., 2005), while at this time there is no recorded deposition in the North St George's Channel Basin (Welch and Turner 2000) and in the Kish Bank Basin (Naylor and Shannon, 2009). Therefore, the Early Cretaceous exhumation is likely to be more regional in extent than the previous Mesozoic exhumation episodes described above and is likely linked to swell-related dynamically support as proposed by Jones et al. (2012). However the amount of uplift generated may be minor, as it is not seen in other profiles in Ireland or Wales. Alternatively, Holford et al. (2005), amongst others, argue that this episode may reflect uplift due to a period of significant extension of the Atlantic Margin and the onset of seafloor spreading in the Bay of Biscay and in the Goban Spur. However this explanation implies a very strong lithosphere, in contradiction to the results of Tiley et al. (2003). Our results cannot readily decipher between these two competing hypotheses.

6.2 Cenozoic thermal history

A second major phase of post-Variscan cooling has occurred in the Early Cenozoic period. The Isle of Arran profile in SW Scotland (Fig. 5b) shows that this Paleocene intrusion achieved surface temperatures shortly after emplacement. This cooling pulse is also evident in individual samples in the Southern Uplands (Fig. 6a) and in northeast Ireland (Fig. 6b). The cooling phase is also detected in the Isle of Man and Snowdonia profiles (Fig. 5a and 3a), and can be detected in individual samples from Anglesey and Pembrokeshire in forward models (Fig. 3b). The two

374 profiles from the Leinster granite (Mount Leinster, Fig. 4b; Lugnaquilla, Fig. 4d) do
375 not show a well-defined rapid pulse of Early Cenozoic cooling, but importantly cooling
376 in both profiles initiated at ca. 60 Ma. This is significantly earlier than the onset of
377 post-Mesozoic cooling in southern Ireland (Galtee Mountains, Fig. 4a), central Ireland
378 (Slieve Bloom; Fig. 4c) and in western Ireland (Cogné et al., 2014), which typically
379 commenced in Neogene times. Therefore this episode of Early Cenozoic cooling is
380 restricted to the margins of the Irish Sea. It starts between ca. 65 and 60 Ma and
381 lasts for ca. 10Ma.
382 We stress here that it is the use of two thermochronometers coupled with a
383 vertical profile approach that allowed us to demonstrate the regional extent of this
384 cooling episode. As shown on Figure 7, the use of AFT data alone for the vertical
385 profile model (Fig. 7b) or modelling individual samples using combined AFT and AHe
386 data (Fig. 7c and 7d) would not detect portions of the cooling history in the studied
387 area. Using two thermochronometers with a vertical profile approach (Fig.7a) not only
388 allowed us to detect this cooling episode, but also to show that it progressively
389 decreases in intensity from north to south and to the west as discussed below.
390
391 *6.3 Spatial distribution of Early Cenozoic cooling*
392 The sampling density in this study does not allow for the construction of a
393 detailed Early Cenozoic cooling map, primarily because analysing multiple samples
394 in a single profile is significantly more time consuming, limiting the spatial density of
395 the resulting data. However, the behaviour of samples in the inverse modelling
396 process can also provide an indication of the intensity of Early Cenozoic cooling, as
397 an Early Cenozoic cooling episode has to be significant to be detected in single
398 samples given that the inversion modelling approach favours simpler solutions.

We can delimit four different areas (Fig. 8) based on the modelled behaviour of single samples and vertical profiles. (i) A significant pulse of Early Cenozoic cooling is present when it is detected by inverse modelling on single samples, and this area runs from the Southern Uplands in SW Scotland to northeast Ireland (red stars on Fig. 8) It also encompasses the prominent cooling pulse detected on the Isle of Arran, but it should be noted that we have not collected a sample from this region outside of the aureole of this Paleocene intrusion. (ii) The second region comprises west Wales and the Isle of Man (orange stars on Fig. 8), where inverse modelling of individual samples does not show the pulse of Early Cenozoic cooling (or is not well constrained as in sample Pb-1 from Pembrokeshire) but where it is detected by inverse modelling of vertical profiles (e.g. the Snowdonia profile). (iii) A third zone in southeast Ireland (yellow stars on Fig. 8) is characterized by vertical profiles that do not show a discrete, rapid pulse of Early Cenozoic cooling, but slow cooling nevertheless initiated at ca. 60 Ma. (iv) The final zone comprises the three profiles in this study (Brecon Beacons, Slieve Bloom and Galtee Mountains) and the five profiles from the western Irish onshore (Cogné et al., 2014) that do not show cooling during the Early Cenozoic (blue stars on Fig. 8).

7. Discussion

7.1 Linking Early Cenozoic cooling to exhumation

We associate the pulse of enhanced Early Cenozoic cooling described above with a pronounced phase of exhumation that has been previously detected in the Irish Sea basin system (e.g., Rowley and White, 1998; Holford et al., 2005). Assuming a paleogeothermal gradient of 25°C/km, similar to the present-day

(Goodman et al., 2004, Downing and Gray, 1986), Early Cenozoic exhumation of ca. 2 km is indicated in the three samples from northeast Ireland, and sample Sct-2 in the NW Southern Uplands (Fig. 8). Early Cenozoic exhumation is most significant in sample Sct-1 (ca. 3 km). This sample is also the only surface sample (excluding the Paleocene Isle of Arran Northern Granite) that yields an Early Cenozoic AFT age in our dataset, indicating that the Early Cenozoic thermal event is more significant in the southwest part of the Southern Uplands than elsewhere in the studied area. Such young AFT ages are relatively uncommon for surface samples in Britain and Ireland, and they tend to be clustered around the NE Irish Sea (e.g. the Vale of Eden, Lewis et al., 1992; Lake District, Green, 2002, East Irish Sea Basin, Lewis et al., 1992; Green et al., 1997). Early studies around the East Irish Sea Basin argued for exhumation of up to 3 km (e.g. Lewis et al., 1992), similar to the exhumation signal we infer for sample Sct-1. However others (e.g. Green et al., 1997) have subsequently argued that the peak temperatures recorded by such samples resulted from a high geothermal gradient. The subsequent cooling history would then only be partly associated with Early Cenozoic exhumation, as there is also a cooling component associated with thermal relaxation from an initial high Early Cenozoic heat flow. Therefore the total amount of denudation is somewhat unclear, but 2.5 to 3 km is within the upper limits of previously published exhumation estimates for the East Irish Sea Basin (Rowley and White, 1998). On the other side of the East Irish Sea Basin, the exhumation inferred for the Isle of Man is lower, at ca. 1.5 km.

The amount of Early Cenozoic exhumation for the Paleocene Isle of Arran Northern Granite is difficult to estimate from low-temperature thermochronology alone, as it cooled rapidly from magmatic temperatures following emplacement. However, maximum exhumation cannot exceed emplacement depth estimates of 2-3

449 km (England, 1992); our data indicate cooling and exhumation was complete by the
450 Early Eocene. Further south in Wales, the amount of Early Cenozoic exhumation is
451 estimated at 1.5 to 2 km based on the cooling histories of the Snowdonia profile and
452 the Anglesey and Pembrokeshire samples. Finally in southeast Ireland, Early
453 Cenozoic exhumation cannot exceed ca. 1-1.5 km, but it is harder to estimate as the
454 Early Cenozoic cooling history is not represented by a discrete cooling pulse.
455
456 *7.2 Causal mechanisms for Early Cenozoic exhumation*
457 Several authors have argued for Cenozoic exhumation caused by localised
458 inversion due to far-field tectonic stress transmission (e.g., Hillis et al., 2008; Holford
459 et al., 2005), but this mechanism is unlikely to be the primary cause for the Early
460 Cenozoic exhumation pattern we document here. The onshore pattern of Early
461 Cenozoic exhumation is not spatially associated with any major faults nor is it limited
462 to belts of known compressive tectonism (Fig. 8). This is not to say that a localised
463 structural control on exhumation is not present; for example, it is required to explain
464 the close spatial proximity (ca. 15 km) of the Late Paleocene Mourne Mountains
465 granite and the Early Paleocene Antrim basalts at similar elevations. However, uplift
466 and exhumation is clearly centred around the Irish Sea, with the maximum amount of
467 exhumation in the north sector (SW Scotland and northeast Ireland) and decreasing
468 towards the south. Moreover, even though Cenozoic crustal shortening is well
469 documented in the southern British Isles, only a subset of this shortening can be
470 attributed to Early Cenozoic movements (Welch and Turner, 2000; Blundell, 2002).
471 Total shortening is an order of magnitude too small to account for the observed
472 exhumation of between 1 to 3 km (Davis et al., 2012). Additionally, if exhumation was
473 controlled by far-field compression then partitioning of shortening onto discrete, brittle

474 crustal structures is expected, together with the formation of structurally-controlled
475 sediment traps hosting Early Cenozoic strata in zones where Early Cenozoic
476 exhumation was minimal to absent. However, the oldest known Cenozoic
477 sedimentary rocks in the Irish Sea basin system comprise the minor Eocene
478 succession in the St George's Channel Basin (Welch and Turner, 2000). Late
479 Cretaceous and Early Paleogene sedimentary rocks are entirely absent in the region,
480 which requires regional-scale exhumation of the entire Irish Sea region during the
481 Early Cenozoic period.

482 Therefore, although structural inversion under compressive stress may have
483 played a secondary role in the observed pattern of Early Cenozoic exhumation, our
484 data demonstrate that this exhumation in and around the Irish Sea region is primarily
485 due to epeirogenic causes. The emplacement of the British-Irish Paleogene Intrusive
486 Province (BIPIP) has been linked to the thermal effects of the proto-Iceland Plume.
487 The BIPIP ranges in age from ca. 63 to 58 Ma (Ganerød et al., 2010) and comprises
488 a series of extrusive and intrusive centres that run from the Outer Hebrides in NW
489 Scotland through the Irish Sea as far south as Lundy (Fig. 8). The Early Cenozoic
490 exhumation pulse thus coincides temporally and spatially with this intense phase of
491 magmatic activity that shortly predates the opening of the North Atlantic at ca. 55 Ma
492 (Rickers et al., 2013). Furthermore, Persano et al. (2007) have argued for a similar
493 episode of Early Cenozoic uplift and exhumation associated with the proto-Iceland
494 plume in western Scotland, while regional-scale Paleocene uplift of northwest Britain
495 and the resultant southeast-directed tilting is in accordance with the outcrop pattern
496 of post-Triassic sedimentary rocks in Britain (Cope, 1994, Fig. 8) and with the
497 provenance of Early Cenozoic sedimentary rocks in the Hampshire basin (Morton,
498 1982). Regional-scale uplift is also in accordance with stratigraphic evidence for large

clastic fan bodies during Paleocene and Eocene times on the margins of the uplifted area (White and Lovell, 1997; Jones et al., 2002; Jones and White, 2003).

Brodie and White (1994) proposed that ca. 5 km of Paleocene magmatic underplating occurred at the base of the crust underlying the Irish Sea region contemporaneous with the emplacement of the BIPIP, which induced sufficient uplift to create regional-scale Paleocene exhumation. Using a wide-angle seismic profile that crossed the Irish Sea, Al-Kindi et al. (2003) imaged an 8 km-thick high velocity zone at the base of the crust underneath the eastern Irish Sea, and which they too interpreted as underplated magmatic material. Tomlinson et al. (2006) refined the shape of this body using seismic receiver function data and their calculated thickness variations are a good match with the spatial distribution of exhumation detected in this study (Fig. 8), and Davis et al. (2012) also argued for the presence of such a high-velocity body beneath Scotland and extending southwards. It is also possible that a component of the observed exhumation pulse was associated with transient and intermittent dynamic uplift induced by the presence of a hot vertical convective sheet in the upper asthenospheric mantle – the presumed source of the underplated material – which would explain the pulsed record of deep-water clastic fans in the Early Cenozoic offshore basins around the British Isles (White and Lovell, 1997, Jones et al., 2002). Following the emplacement of the BIPIP, a second phase of transient uplift that encompassed a large part of the British Isles occurred at the Paleocene / Eocene boundary, and is linked to the presence of a hot horizontal layer beneath the lithosphere (Jones and White, 2003). Both processes could have caused a significant portion of the Paleocene exhumation documented here. Although the spatial distribution of Paleocene exhumation (centred along a north-south axis under the Irish Sea) tends to favour the vertical convective sheet model, the temporal

sensitivity of our low-temperature thermochronological data also allows for a more widespread (but more subtle, at least in Ireland) phase of transient uplift as proposed by Jones and White (2003). In any case, both mechanisms are linked to plume-related (i.e. epeirogenic) regional-scale exhumation during the Early Cenozoic.

Following the Early Cenozoic exhumation phase, the thermal history models indicate that some parts of onshore Ireland and Britain may have undergone a final limited phase of cooling (< ca. 30°C) during the Neogene period. A similar-magnitude pulse of reheating often predates this cooling episode. However, the thermal history models are not sensitive at temperatures below ca. 40°C, as these temperatures are cooler than the lower temperature limits of both the AHe and particularly the AFT techniques. Nonetheless, Neogene uplift and exhumation of some parts of the British Isles driven by plume-related processes is in agreement with the proposal that the present-day topography of the British Isles is dynamically supported (e.g. Jones et al., 2002; Davis et al., 2012; Rickers et al., 2013), and with the reported presence of a “finger” of anomalously hot asthenosphere propagating from the Iceland plume towards the Irish Sea region. The latter is visible in the upper asthenospheric mantle on seismic tomographic images at depths of ca. 120 to 160 km (Arrowsmith et al., 2005; Rickers et al., 2013).

8. Conclusions

The use of two low-temperature thermochronometers (the AFT and AHe systems) combined with a vertical profile sampling approach and inverse and forward modelling, allows us to define the cooling history of the British Isles, and especially the Irish Sea region, with hitherto unparalleled resolution. From end Permian to

549 Jurassic times, exhumation was likely linked to the uplift and erosion of the hinterland
550 during the complex and long-lived rifting history of the region, with each profile
551 recording a cooling phase synchronous with the major phase of rifting in the nearest
552 offshore basin. It is possible that during the Early Cretaceous period, transient
553 dynamic uplift was responsible for exhumation detected in two of our profiles,
554 although more work is needed to confirm this hypothesis. An Early Cenozoic pulse of
555 exhumation affected the onshore margins of the Irish Sea basin system, and is more
556 significant in the north (reaching ca. 2.5-3 km), decreasing in intensity towards the
557 south and west. Combined with the available geophysical and sedimentological
558 evidence, we demonstrate that the main cause of this regional-scale uplift and
559 exhumation is linked to the effects of the proto-Iceland plume. A body of magmatic
560 material emplaced into the base of the lower crust and which broadly corresponds in
561 seismic studies to the present-day limits of the BIPIP is likely to be the main causal
562 mechanism. It is also possible that transient dynamic support was responsible for a
563 component of the observed Early Cenozoic exhumation, while local reactivation
564 along discrete structures can account for local variations in the observed exhumation
565 pattern in the region. Subsequently, the late Cenozoic thermal history evolution of the
566 British Isles remains under-constrained, but a second phase of Neogene plume-
567 linked exhumation is possible.

568 The combination of AFT and AHe dating with vertical profile modelling has
569 proven key in resolving the hitherto disparate cooling histories documented in the
570 Irish Sea region during the Early Cenozoic. Persano et al. (2007) detected Early
571 Cenozoic underplating-driven uplift and denudation in western Scotland using a
572 similar approach; in both regions single-sample modelling of AFT data alone would
573 fail to detect the Early Cenozoic exhumation pulse (cf Fig. 7). Further AHe

thermochronology from vertical profiles on onshore Britain would more precisely constrain the region of influence of the proto-Iceland plume during the Early Cenozoic.

Our data supports the hypothesis that the Early Cenozoic exhumation history of the British Isles is linked to the presence of the Iceland Plume. The spatial distribution of the BIPIP onshore follows the same axis as the distribution of exhumation from the Outer Hebrides to Lundy Island. It is therefore likely that the presence of abnormally hot vertical sheet of mantle centred below the Irish Sea explains the relatively short wavelength of early Paleocene exhumation inferred for the British Isles; seismic tomographic data suggest a similar situation may exist today (Rickers et al., 2013).

Acknowledgments

NC and DC thank Science Foundation Ireland who part-funded this work under Grant Number 13/RC/2092 (iCRAG Research Centre, project HC4.2PD6a). iCRAG is funded under the SFI Research Centres Programme and is co-funded under the European Regional Development Fund. DD is funded under The Earth and Natural Sciences Doctoral Studies Program, which is funded under the Program for Research in Third-Level Institutions and co-funded under the European Regional Development Fund. We thank S. Jones and an anonymous reviewer for their comments that significantly improved the manuscript. We would also like to thank S. Lebedev and colleagues in the Dublin Institute of Advanced Studies for many useful discussions.

References

599 Al Kindi, S., White, N.J., Sinha, M., England, R.W. & Tiley, R., 2003. The crustal
600 trace of a hot convective sheet, Geology, 31, 207–210.

601 Allen, P.A., Bennett, S.D., Cunningham, M.J.M., Carter, A., Gallagher, K.,
602 Lazzaretti, E., Galewsky, J., Densmore, A.L., Phillips, W.E.A., Naylor, D., Hach, C.S.,
603 2002. The post-Variscan thermal and denudational history of Ireland. in: Doré, A.G.,
604 Cartwright, M.S., Stoker, M.S., Turner, J.P., White, N. (Eds.). Exhumation of the
605 North Atlantic margin: timing, mechanisms and implications for the petroleum
606 exploration. Geological Society, London, Special Publications, 196, 371-399.

607 Arrowsmith, S.J., Kendall, M., White, N., VanDecar, J.C. & Booth, D.C., 2005.
608 Seismic imaging of a hot upwelling beneath the British Isles, Geology, 33(5), 345–
609 348.

610 Blundell, D.J., 2002. Cenozoic inversion and uplift of Southern Britain, in
611 Exhumation of the North Atlantic Margin: Timing, Mechanisms and Implications for
612 Petroleum Exploration, in: Doré, A.G., Cartwright, M.S., Stoker, M.S., Turner, J.P.,
613 White, N. (Eds.). Exhumation of the North Atlantic margin: timing, mechanisms and
614 implications for the petroleum exploration. Geological Society, London, Special
615 Publications, 196, 85-101.

616 Braun, J., 2010. The many surface expressions of mantle dynamics. Nature
617 Geosciences 3, 825-833.

618 Brodie, J., White, N., 1994. Sedimentary basin inversion caused by igneous
619 underplating: Northwest European continental shelf. Geology 22, 147-150.

620 Burov, E., Cloetingh, S., 2009. Controls of mantle plumes and lithospheric folding
621 on modes of intraplate continental tectonics: differences and similarities. Geophysical
622 Journal International 178, 1691-1722.

623 Chew, D.M., Petrus, J.A., Kamber, B.S., 2014. U-Pb LA-ICPMS dating using
624 accessory mineral standards with variable common Pb. Chemical Geology 363, 185-
625 199.

626 Cogné, N., Chew, D.M., Stuart, F.M., 2014. The thermal history of the western
627 Irish onshore. Journal of the Geological Society, 171, 779-792.

628 Cope, J.C.W, 1994. A latest Cretaceous hotspot and the Southeasterly tilt of
629 Britain. Journal of the Geological Society 151, 905-908.

630 Cox, K., 1989, The role of mantle plumes in the development of continental
631 drainage patterns. Nature 342, 873–877.

632 Davis, M.W., White, N.J., Priestley, K.F., Baptie B. J., Tilmann F.J., 2012. Crustal
633 structure of the British Isles and its epeirogenic consequences. Geophysical Journal
634 International 190, 705-725.

635 Donelick, R.A., O'Sullivan, P.B., Ketcham, R.A., 2005. Apatite Fission-Track
636 Analysis. Reviews in Mineralogy and Geochemistry 58, 49-94.

637 Downing, R.A., Gray, D.A., 1986. Geothermal resources of the United Kingdom.
638 Journal of the Geological Society 143 , 499-507.

639 England, R.W., 1992. The genesis, ascent, and emplacement of the Northern
640 Arran Granite, Scotland: Implications for granitic diapirism. Geological Society of
641 America Bulletin 104, 606-614.

642 Flowers, R.M., Ketcham, R.A., Shuster, D.L., Farley, K.A., 2009. Apatite (U-
643 Th)/He thermochronometry using a radiation damage accumulation and annealing
644 model. Geochimica et Cosmochimica Acta 73, 2347-2365.

645 Foeken, J.P.T., Stuart, F.M., Dobson, K.J., Persano, C., Vilbert, D., 2006. A
646 diode laser system for heating minerals for (U-Th)/He chronometry. Geochemistry,
647 Geophysics, and Geosystems 7, Q04015.

648 Gallagher, K., 1995. Evolving temperature histories from apatite fission-track
649 data. Earth and Planetary Science Letters 136, 421-435.

650 Gallagher, K., 2012. Transdimensional inverse thermal history modeling for
651 quantitative thermochronology. Journal of Geophysical Research 117, B02408.

652 Gallagher, K., Stephenson, J., Brown, R., Holmes, C., Fitzgerald, P., 2005. Low
653 temperature thermochronology and modeling strategies for multiple samples 1:
654 Vertical profiles. Earth and Planetary Science Letters 237, 193-208.

655 Ganerød, M., Smethurst, M.A., Torsvik, T.H., Prestvik, T., Rousse, S., McKenna,
656 C., van Hinsbergen, D.J.J., Hendriks, B.W.H., 2010. The North Atlantic Igneous
657 Province reconstructed and its relation to the Plume Generation Zone: the Antrim
658 Lava Group revisited. Geophysical Journal International 182, 183-202.

659 Goodman, R., G.L., J., Kelly, J., Slowey, E., O'Neill, N., 2004. Geothermal
660 Energy Resource Map of Ireland. Final Report.

661 Green, P. F. 2002. Early Tertiary paleo-thermal effects in Northern England:
662 reconciling results from apatite fission track analysis with geological evidence.
663 Tectonophysics 349, 131–144.

664 Green, P. F., Duddy, I. R. & Bray, R. J. 1997. Variation in thermal history styles
665 around the Irish Sea and adjacent areas: implications for hydrocarbon occurrence
666 and tectonic evolution. In: Meadows, N. S., Trueblood, S. P., Hardman, M. & Cowan,
667 G. (eds) Petroleum Geology of the Irish Sea and Adjacent Areas. Geological Society,
668 London, Special Publications, 124, 73–93.

669 Green, P.F., Duddy, I.R., Hegarty, K.A., Bray, R.J., Sevastopulo, G., Clayton, G.,
670 Johnston, D., 2000. The post-Carboniferous evolution of Ireland: evidence from
671 Thermal History Reconstruction. Proceedings of the Geologists' Association 111,
672 307-320.

673 Green, P.F., Crowhurst, P.V., Duddy, I.R., Japsen, P., Holford, S.P., 2006.
674 Conflicting (U-Th)/He and fission track ages in apatite: Enhanced He retention, not
675 anomalous annealing behaviour. Earth and Planetary Science Letters 250, 407-427.

676 Hillis, R.R., Holford, S.P., Green, P.F., Doré, A.G., Gatliff, R.W., Stoker, M.S.,
677 Thomson, K., Turner, J.P., Underhill, J.R., Williams, G.A., 2008. Cenozoic
678 exhumation of the southern British Isles. Geology 36, 371-374.

679 Holford, S.P., Turner, J.P., Green, P.F., 2005. Reconstructing the Mesozoic -
680 Cenozoic exhumation history of the Irish Sea basin system using apatite fission track
681 analysis and vitrinite reflectance data. Geological Society, London Petroleum
682 Geology Conference series 6, 1095-1107.

683 Jones, S., White, N., Clarke, B.J., Rowley, E., Gallagher, K., 2002. Present and
684 past influence of the Iceland Plume on sedimentation, in: Doré, A.G., Cartwright,
685 M.S., Stoker, M.S., Turner, J.P., White, N. (Eds.). Exhumation of the North Atlantic
686 margin: timing, mechanisms and implications for the petroleum exploration.
687 Geological Society, London, Special Publications, 196, 13-25.

688 Jones, S.M., Lovell, B., Crosby, A.G., 2012. Comparison of modern and
689 geological observations of dynamic support from mantle convection. Journal of the
690 Geological Society 169 , 745-758.

691 Jones, S.M., White, N., 2003. Shape and size of the starting Iceland plume swell,
692 Earth and Planetary Science Letters 216, 271–282.

693 Kamerling, P., 1979. The geology and hydrocarbon habitat of the Bristol Channel
694 Basin. Journal of Petroleum Geology 2, 75-93.

695 Ketcham, R.A., Carter, A., Donelick, R.A., Barbarand, J., Hurford, A.J., 2007.
696 Improved modeling of fission-track annealing in apatite. American Mineralogist 92,
697 799-810.

698 Lewis, C. L. E., Green, P. F., Carter, A., Hurford, A. J. 1992. Elevated K/T
699 palaeotemperatures throughout Northwest England: three kilometres of Tertiary
700 erosion? Earth and Planetary Science Letters 112, 131 – 145.

701 Meesters, A.G.C.A., Dunai, T.J., 2002. Solving the production-diffusion equation
702 for finite diffusion domains of various shapes: Part II. Application to cases with
703 [alpha]-ejection and nonhomogeneous distribution of the source. Chemical Geology
704 186, 57-73.

705 Morton, A.C., 1982. Heavy minerals of Hampshire Basin Paleogene strata.
706 Geological Magazine, 119, 463-476.

707 Naylor, D., Shannon, P.M., 2009. Geology of Offshore Ireland, in: Holland, C.H.,
708 Sander, I.S. (Eds.). The geology of Ireland, 2nd edition. Dunedin Academic Press ltd,
709 Edinburgh, Scotland, pp. 405-460.

710 Persano, C., Barfod, D.N., Stuart, F.M., Bishop, P., 2007. Constraints on early
711 Cenozoic underplating-driven uplift and denudation of western Scotland from low
712 temperature thermochronometry. Earth and Planetary Science Letters 263, 404-419.

713 Rickers, F., Fichtner, A., Trampert, J., 2013. The Iceland–Jan Mayen plume
714 system and its impact on mantle dynamics in the North Atlantic region: Evidence
715 from full-waveform inversion. Earth and Planetary Science Letters 367, 39-51.

716 Rowley, E., White, N., 1998. Inverse modelling of extension and denudation in
717 the East Irish Sea and surrounding areas. Earth and Planetary Science Letters, 161,
718 57-71.

719 Shuster, D.L., Farley, K.A., 2009. The influence of artificial radiation damage and
720 thermal annealing on helium diffusion kinetics in apatite. Geochimica et
721 Cosmochimica Acta 73, 183-196.

722 Simms, M.J., 2009. Permian and Mesozoic, in: Holland, C.H., Sander, I.S. (Eds.).
723 The Geology of Ireland, 2nd edition. Dunedin Academic Press, Edinburgh, Scotland,
724 pp. 311-332.

725 Stuart, F.M., Ellam, R.M., Harrop, P.J., Fitton, J.G., Bell, B.R., 2000. Constraints
726 on mantle plumes from the helium isotopic composition of basalts from the
727 British Tertiary Igneous Province. Earth and Planetary Science Letters 177, 273-285.

728 Tiley, R., McKenzie D., White, N., 2003. The elastic thickness of the British Isles.
729 Journal of the Geological Society 160, 499 – 502.

730 Tomlinson, J.P., Denton, P., Maguire, P.K.H., Booth, D.C., 2006. Analysis of the
731 crustal velocity structure of the British Isles using teleseismic receiver functions.
732 Geophysical Journal International 167, 223-237.

733 Welch, M.J. & Turner, J.P. 2000. Triassic – Jurassic development of the St.
734 George's Channel basin, offshore Wales, UK. Marine and Petroleum Geology, 17(6),
735 723–750.

736 Williams, G.A., Turner, J. P., Holford, S. P., 2005. Inversion and exhumation of
737 the St George's Channel Basin, offshore Wales, UK. Journal of the Geological
738 Society 162, 97 – 110.

739 White, N., McKenzie, D., 1989. Magmatism at rift zones: the generation of
740 volcanic continental margins and flood basalts. Journal of Geophysical Research 94,
741 7685-77729.

742 White, N., Lovell, B., 1997. Measuring the pulse of a plume with the sedimentary
743 record. Nature 387, 888-891.

744 Ziegler, P.A., Cloetingh, S., and van Wees, J.-D., 1995. Dynamics of intra-plate
745 compressional deformation: The Alpine foreland and other examples:
746 Tectonophysics, 252, 7–59.

747

748

749 **Figure Captions**

750

751 Table 1: Fission track results.

752 [1]Lithology: Grt = Granitoid intrusion; Sst = Sandstone. Age: Camb = Cambrian; LDev
753 = Lower Devonian; Ord = Ordovician; Pal = Paleogene; PreC = Precambrian; UDev =
754 Upper Devonian.

755 [2]Number of counted spontaneous tracks.

756 [3]Sum of the individual grain $^{238}U/^{43}Ca$ ratios measured by ICPMS and weighted by
757 the counted area.

758 [4]Counted area.

759 [5] Constraint used for the inverse modelling: DA = Deposition age; EA = Emplacement
760 age; UPb = apatite U-Pb age (unpublished); VM = Variscan metamorphism

761

762 Table 2: (U-Th-Sm/He) results

763

764 Figure 1: Topographic map of the studied area showing the sample locations and the
765 localities discussed in the text. Inset: Location of the studied area on the Northwest
766 European margin.

767

768 Figure 2: Plot of F_T-corrected (U-Th-Sm)/He *vs* AFT ages. The grey bars show the
769 timing of emplacement of the British-Irish Tertiary Igneous Province.

Figure 3: Thermal history models from Wales. The black boxes are user-specified temperature-time constraints. (a) Inverse model for the Snowdonia profile; (b) Inverse and forward models for individual samples from Anglesey and Pembrokeshire; (c) Inverse model for the Brecon Beacons profile.

Figure 4: Thermal history models of pseudo-vertical profiles from SE Ireland. The black boxes are user-specified temperature-time constraints. (a) Galtee Mountains; (b) Mount Leinster; (c) Slieve Bloom and (d) Lugnaquilla.

Figure 5: Thermal history models from the Isle of Man and Isle of Arran. The black boxes are user-specified temperature-time constraints. (a) Inverse and forward modelling of the Isle of Man profile; (b) Isle of Arran profile.

Figure 6: Thermal history models for Southern Uplands and northeast Ireland. The black boxes are user-specified temperature-time constraints. (a) Individual samples Sct-1 and Sct-2; (b) Inverse modelling of individual samples Ire-8, Ire-9 and Ire-10.

Figure 7: Comparison of thermal history models for the Snowdonia profile using thermochronological data from individual versus multiple samples. (a) Model with AFT and AHe data from three samples modelled using the vertical profile approach (as presented in Fig. 3a); (b) Model with AFT data *only* from three samples modelled with the vertical profile approach; (c) Model with AFT and AHe data for sample Cu-3 *only*; (d) Model with AFT and AHe data for sample Cu-4 *only*. The model for Cu-2

794 *only* is similar to the two other two individual samples (Cu-3,-4) and is presented in
795 supplementary material with the predictions.
796
797 Figure 8: Map of Britain and Ireland showing the spatial distribution of Early Cenozoic
798 exhumation phase inferred from our low-temperature thermochronological data and
799 its spatial relationship with the postulated region of magmatic underplating. The main
800 zones of Early Cenozoic deformation along with outcrops of post-Triassic
801 sedimentary rocks and the British-Irish Paleogene Igneous Province are also
802 illustrated.

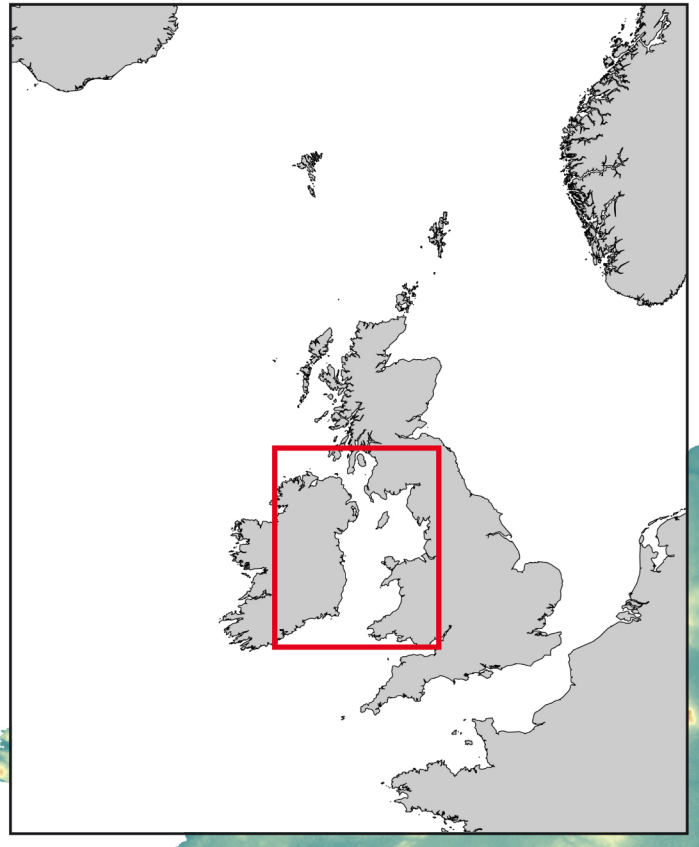

Arran
Sct-2
Sct-1
3°W
55.5°N
Ulster Basin
Solway Firth Basin
Vale of Eden
Lake District
IoM-1
IoM-2
IoM-3
Ire-9
Ire-8
Ire-10 (-1702m)
East Irish Sea Basin
An-1
Cheshire Basin
Kish Bank Basin
LG17
LG18
LG19
Slieve Bloom
Lugnaquilla
LG32
Snowdonia
Cardigan Bay Basin
Mount Leinster
Central Irish Sea Basin
Galtee Mountains
St Georges Channel Basin
Bg-1
Brecon Beacons
Pb-1
Pb-2
Elevation
1345 m
0 m
Vertical profile (multiple samples)
Individual sample
100 km
Celtic Sea Basin
8°W
51.5°N
51.5°N
4°W
Bristol Channel Basin

Figure 2

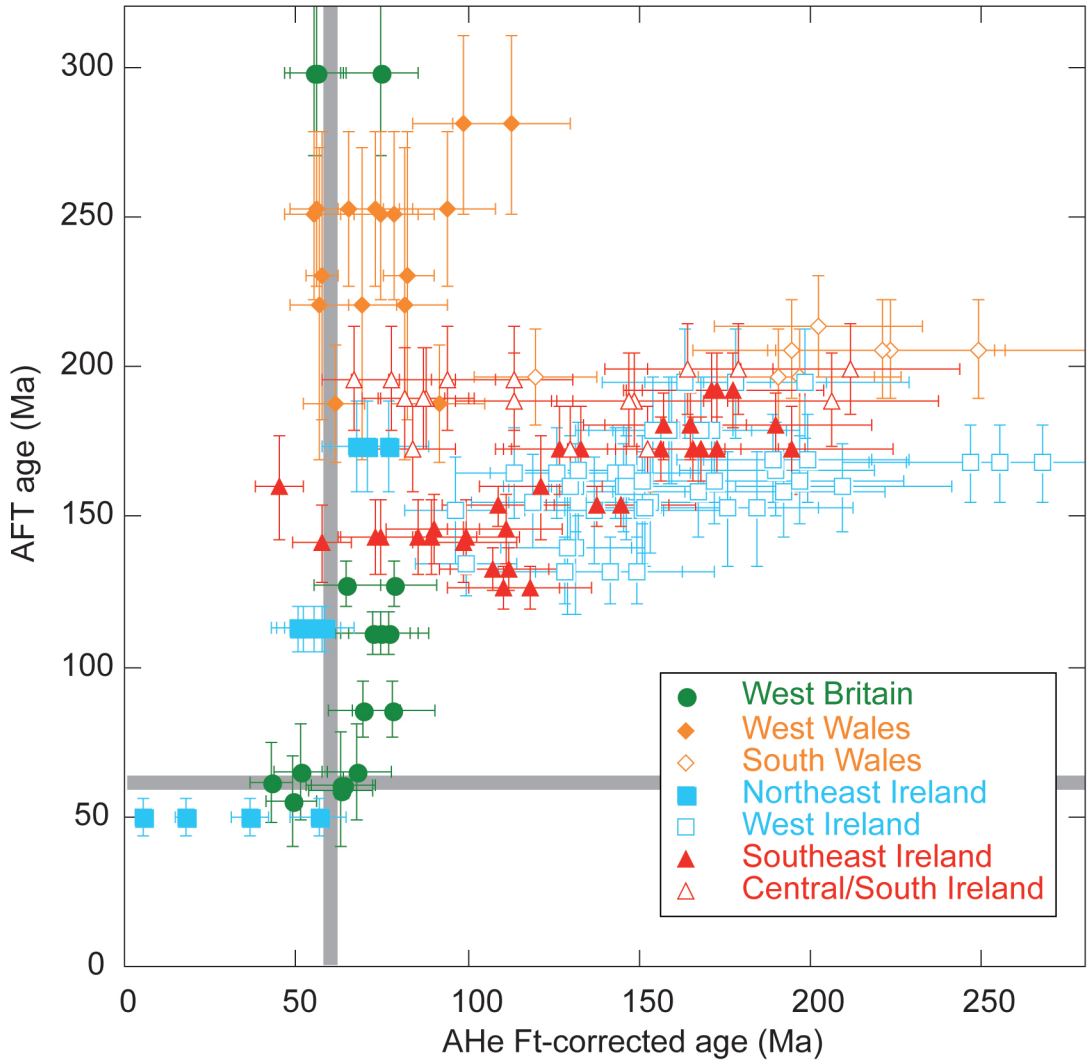
AFT age (Ma)
AHe Ft-corrected age (Ma)
0
50
100
150
200
250
300
West Britain
West Wales
South Wales
Northeast Ireland
West Ireland
Southeast Ireland
Central/South Ireland

Figure 3

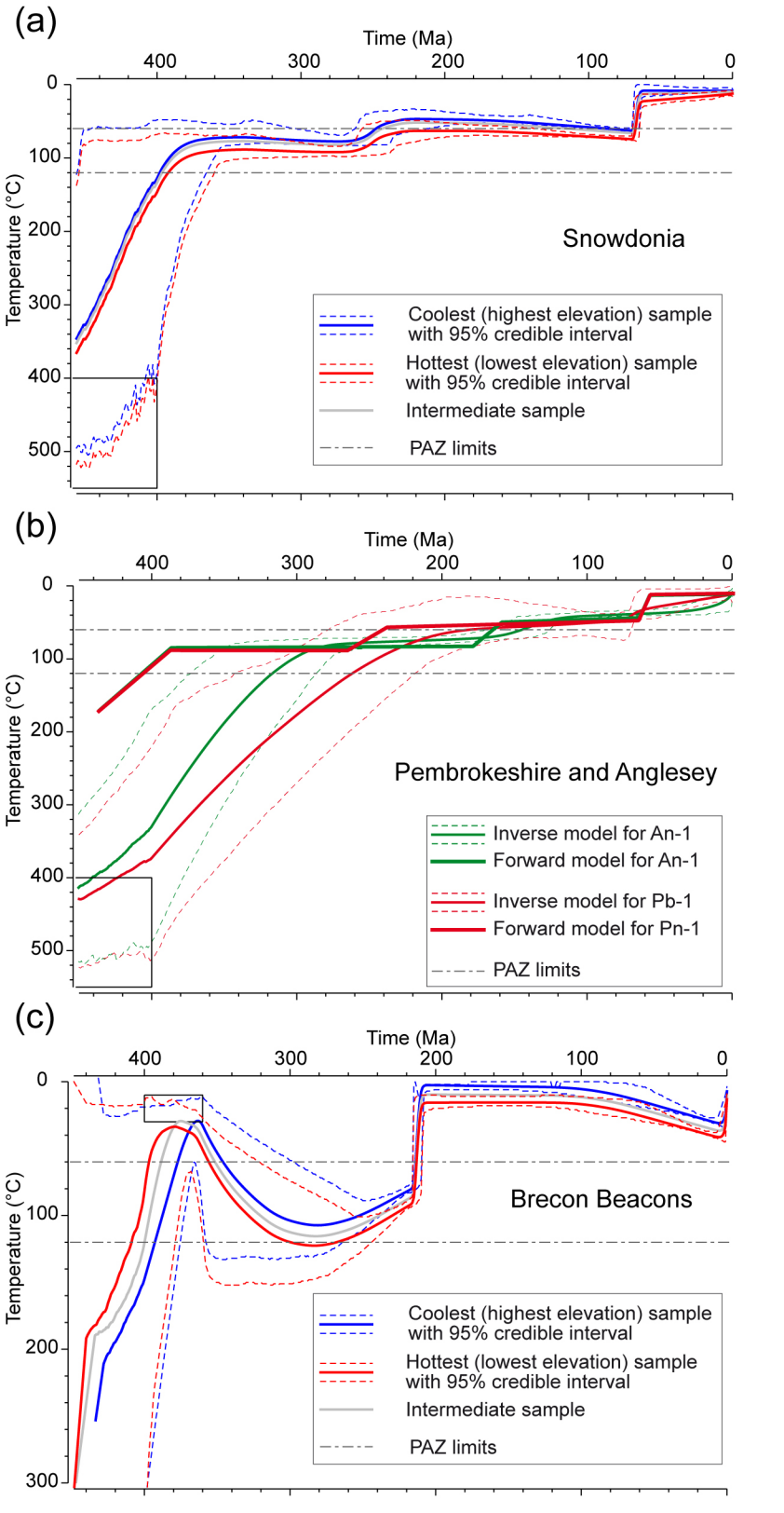
(a)
Time (Ma)
400
300
200
100
0
Temperature (°C)
0
100
200
300
400
500
Snowdonia
Coolest (highest elevation) sample with 95% credible interval
Hottest (lowest elevation) sample with 95% credible interval
Intermediate sample
PAZ limits
(b)
Time (Ma)
Temperature (°C)
Pembrokeshire and Anglesey
Inverse model for An-1
Forward model for An-1
Inverse model for Pb-1
Forward model for Pn-1
PAZ limits
(c)
Time (Ma)
Temperature (°C)
Brecon Beacons
Coolest (highest elevation) sample with 95% credible interval
Hottest (lowest elevation) sample with 95% credible interval
Intermediate sample
PAZ limits

Figure 4

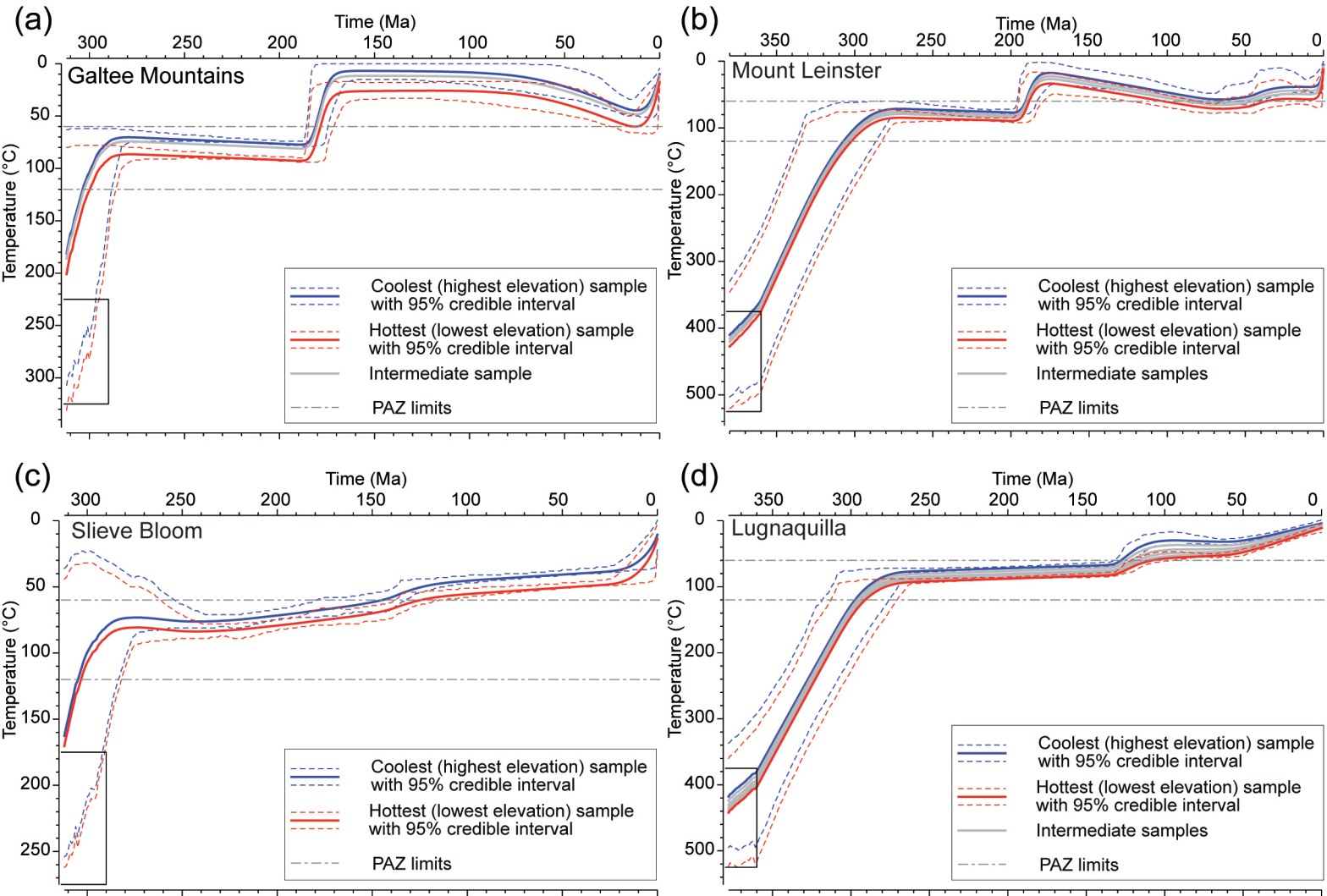
(a)
Galtee Mountains
Time (Ma)
Temperature (°C)
Coolest (highest elevation) sample with 95% credible interval
Hottest (lowest elevation) sample with 95% credible interval
Intermediate sample
PAZ limits
(b)
Mount Leinster
Time (Ma)
Temperature (°C)
Coolest (highest elevation) sample with 95% credible interval
Hottest (lowest elevation) sample with 95% credible interval
Intermediate samples
PAZ limits
(c)
Slieve Bloom
Time (Ma)
Temperature (°C)
Coolest (highest elevation) sample with 95% credible interval
Hottest (lowest elevation) sample with 95% credible interval
PAZ limits
(d)
Lugnaquilla
Time (Ma)
Temperature (°C)
Coolest (highest elevation) sample with 95% credible interval
Hottest (lowest elevation) sample with 95% credible interval
Intermediate samples
PAZ limits

Figure 5

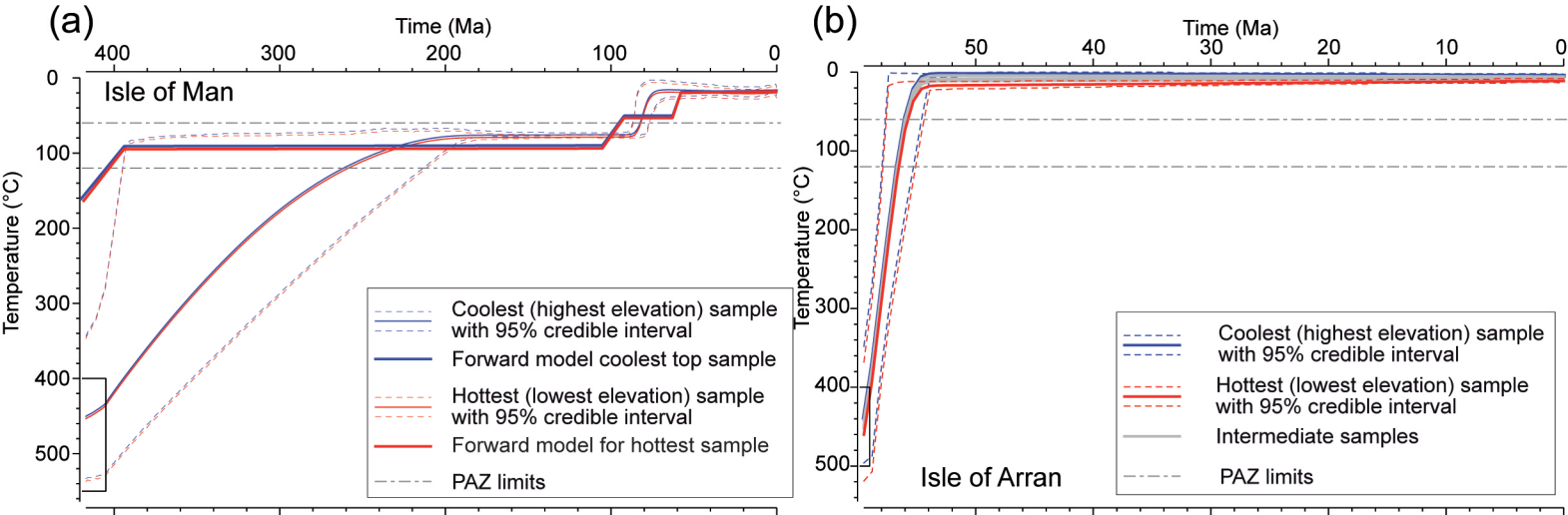
(a)
Time (Ma)
400
300
200
100
0
Isle of Man
Temperature (°C)
0
100
200
300
400
500
Coolest (highest elevation) sample with 95% credible interval
Forward model coolest top sample
Hottest (lowest elevation) sample with 95% credible interval
Forward model for hottest sample
PAZ limits
(b)
Time (Ma)
50
40
30
20
10
0
Isle of Arran
Temperature (°C)
0
100
200
300
400
500
Coolest (highest elevation) sample with 95% credible interval
Hottest (lowest elevation) sample with 95% credible interval
Intermediate samples
PAZ limits

Figure 6

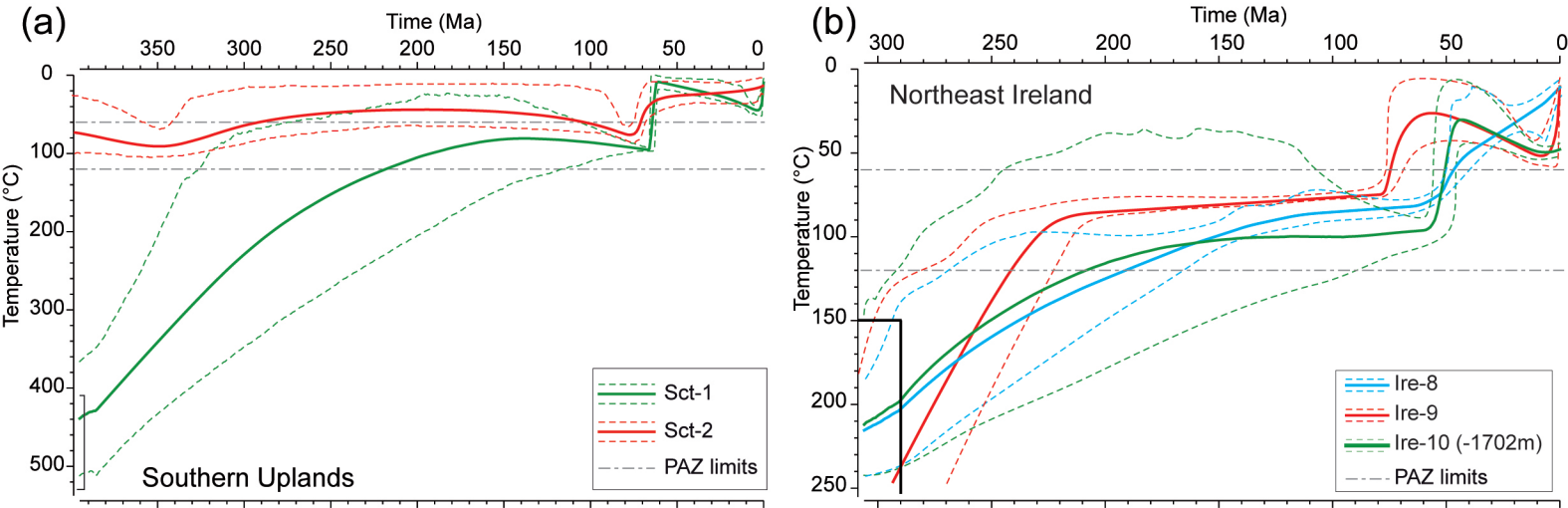
(a)
Time (Ma)
350
300
250
200
150
100
50
0
Temperature (°C)
0
100
200
300
400
500
Sct-1
Sct-2
PAZ limits
Southern Uplands
(b)
Time (Ma)
300
250
200
150
100
50
0
Temperature (°C)
0
50
100
150
200
250
Northeast Ireland
Ire-8
Ire-9
Ire-10 (-1702m)
PAZ limits

Figure 7

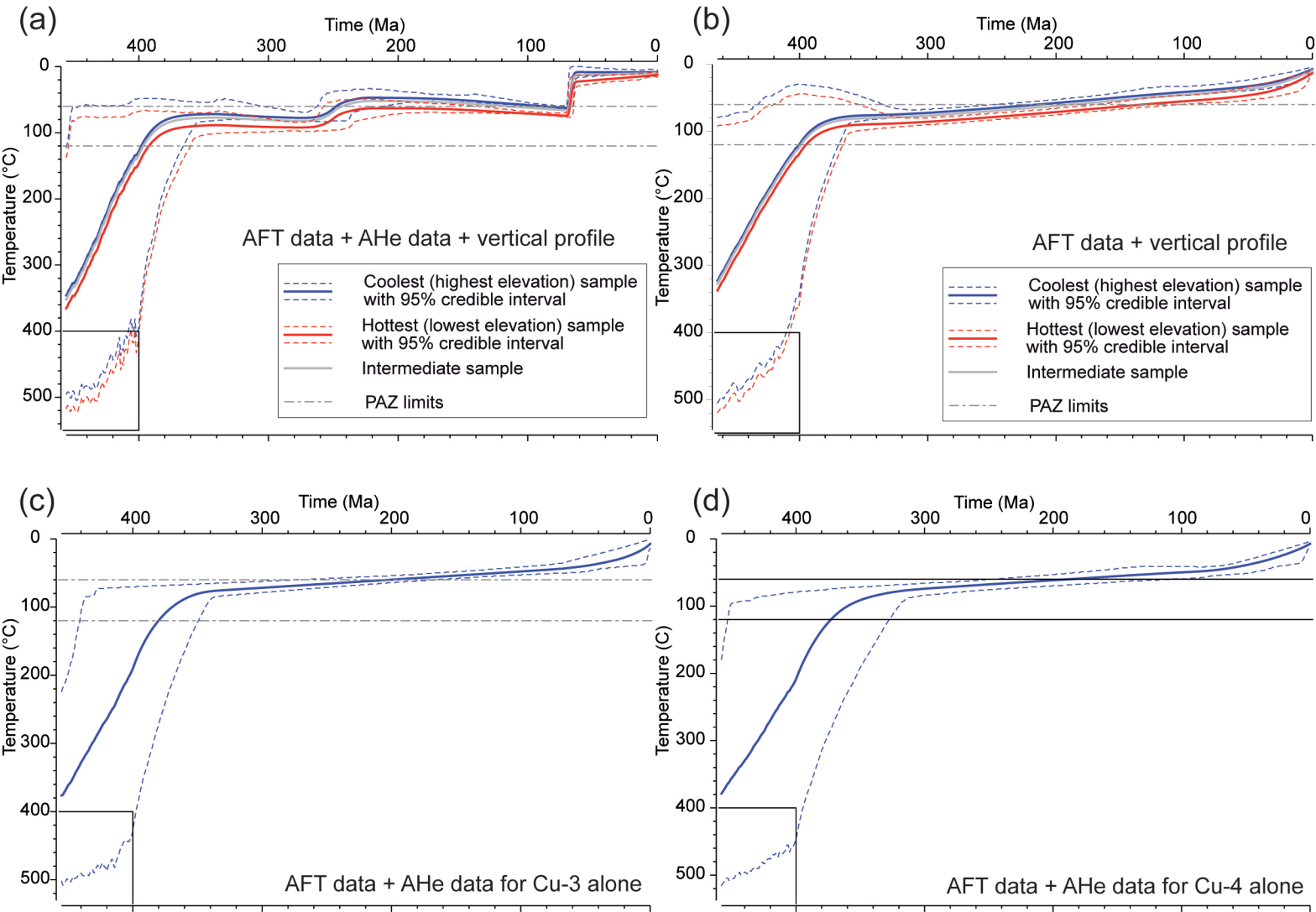
(a)
Time (Ma)
400
300
200
100
0
Temperature (°C)
0
100
200
300
400
500
AFT data + AHe data + vertical profile
Coolest (highest elevation) sample with 95% credible interval
Hottest (lowest elevation) sample with 95% credible interval
Intermediate sample
PAZ limits
(b)
Time (Ma)
AFT data + vertical profile
Coolest (highest elevation) sample with 95% credible interval
Hottest (lowest elevation) sample with 95% credible interval
Intermediate sample
PAZ limits
(c)
Time (Ma)
Temperature (°C)
AFT data + AHe data for Cu-3 alone
(d)
Time (Ma)
Temperature (C)
AFT data + AHe data for Cu-4 alone

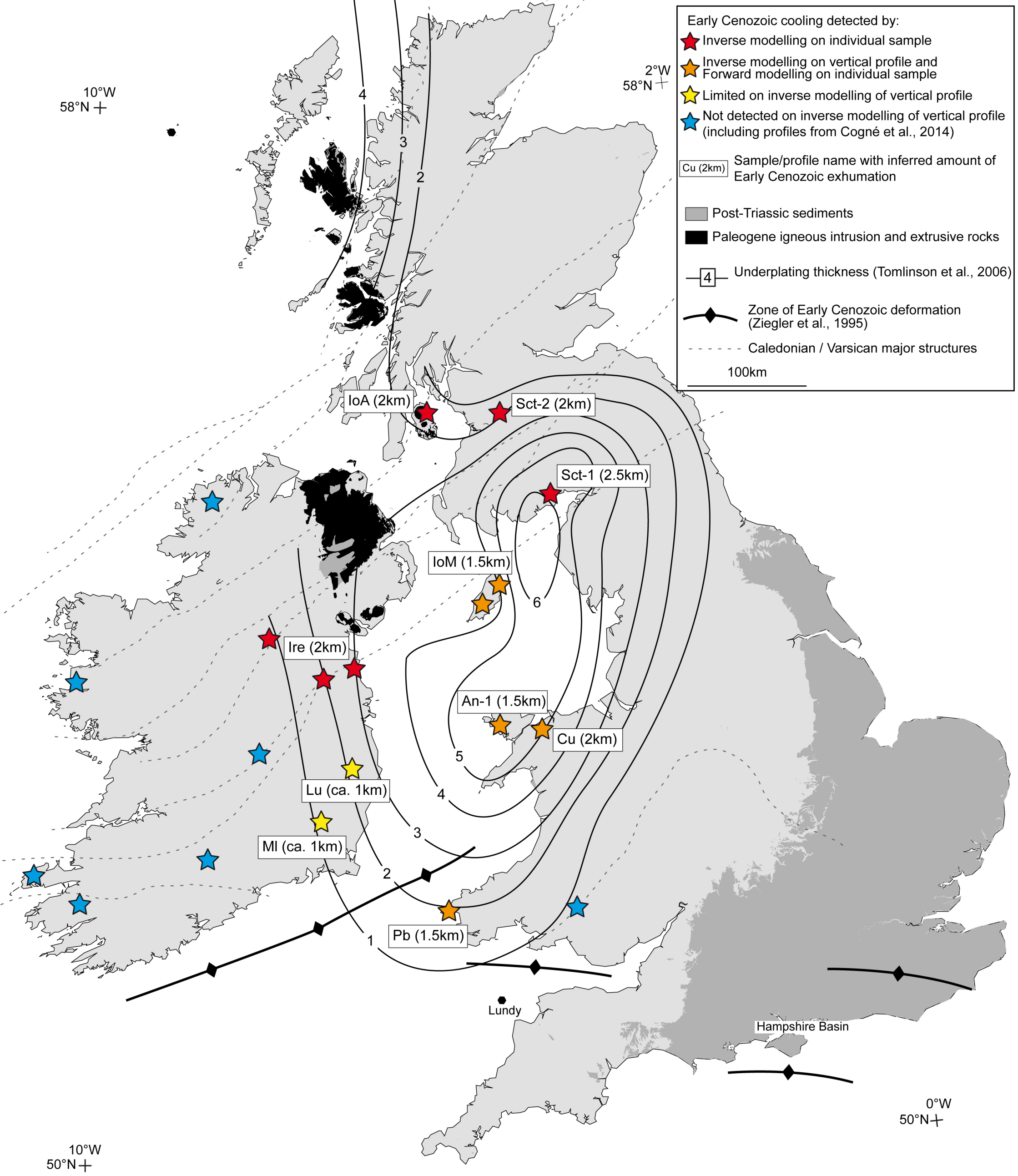
Early Cenozoic cooling detected by:
Inverse modelling on individual sample
Inverse modelling on vertical profile and Forward modelling on individual sample
Limited on inverse modelling of vertical profile
Not detected on inverse modelling of vertical profile (including profiles from Cogné et al., 2014)
Cu (2km)
Sample/profile name with inferred amount of Early Cenozoic exhumation
Post-Triassic sediments
Paleogene igneous intrusion and extrusive rocks
4
Underplating thickness (Tomlinson et al., 2006)
Zone of Early Cenozoic deformation (Ziegler et al., 1995)
Caledonian / Varsican major structures
100km
10°W
58°N
2°W
58°N
10°W
50°N
0°W
50°N
IoA (2km)
Sct-2 (2km)
Sct-1 (2.5km)
IoM (1.5km)
Ire (2km)
An-1 (1.5km)
Cu (2km)
Lu (ca. 1km)
Ml (ca. 1km)
Pb (1.5km)
1
2
3
4
5
6
Lundy
Hampshire Basin

Sample Name	Latitude (°N)	Longitude (°W)	Elevation	Lithology and Stratigraphic age[1]	Ns[2]	238U/43Ca[3]	Area (cm^2)[4]	AFT age (Ma)	± 2σ (Ma)	# grains	P(χ^2)	MTL (μm)	SE (μm)	SD (μm)	# tracks	Dpar (μm)	SE (μm)	Tt constraint[5]
Northeast Ireland																		
Ire 8	53.716	6.329	3	Grt (Low Dev)	1657	1.49E-04	8.61E-04	112.8	7.8	20	0.07	13.4	0.22	1.47	100	2.01	0.27	VM
Ire 9	53.953	7.441	120	Grt (Low Dev)	1018	5.74E-05	8.01E-04	173.4	14.4	22	0.83	13.7	0.17	1.09	101	1.78	0.19	VM
Ire 10	53.639	6.706	-1702	Grt (Low Dev)	358	7.07E-05	4.68E-04	50.0	5.8	29	0.76	13.9	0.41	1.34	17	1.89	0.44	VM
Central/South Ireland																		
Bg-1	52.063	8.695	162	Sdt (Up Dev)	826	4.65E-05	4.03E-04	188.9	15.4	30	0.11	13.0	0.25	1.43	100	1.64	0.18	VM
Galtee Mountains Profile																		
Ga-1	52.366	8.182	909	Sdt (Up Dev)	997	5.35E-05	3.25E-04	199.4	15.2	28	0.05	13.5	0.25	1.42	103	1.59	0.21	VM
Ga-2	52.358	8.187	731	Sdt (Up Dev)	966	5.25E-05	3.60E-04	182.5	15.2	29	0.09	13.3	0.25	1.56	102	1.60	0.17	VM
Ga-4	52.321	8.176	183	Sdt (Up Dev)	870	4.69E-05	3.48E-04	172.5	14.4	28	0.1	13.3	0.23	1.42	115	1.61	0.18	VM
Slieve Bloom Profile																		
Sb-1	53.092	7.557	437	Sdt (Up Dev)	676	3.47E-05	4.01E-04	189.6	17.0	28	0.12	13.6	0.22	1.31	100	1.68	0.19	VM
Sb-3	53.138	7.528	142	Sdt (Up Dev)	550	2.75E-05	4.31E-04	195.9	17.6	29	0.13	13.3	0.21	1.42	102	1.64	0.21	VM
Southeast Ireland																		
LG17	53.087	6.370	517	Grt (Low Dev)	2601	1.68E-04	1.07E-03	153.6	9.6	21	0.09	13.6	0.20	1.06	103	1.55	0.15	UPb
LG18	53.087	6.362	553	Grt (Low Dev)	3125	2.34E-04	1.22E-03	132.9	7.2	22	0.12	13.7	0.19	1.16	102	1.55	0.18	UPb
LG19	53.066	6.337	389	Grt (Low Dev)	2556	2.01E-04	1.24E-03	126.5	7.0	21	0.08	13.8	0.18	1.22	100	1.52	0.21	UPb
LG32	52.804	6.717	122	Grt (Low Dev)	459	3.12E-05	1.16E-03	145.9	15.0	20	0.10	13.0	0.20	1.19	100	1.53	0.22	UPb
Lugnaquilla Profile																		
Lu-1	52.970	6.460	901	Grt (Low Dev)	608	3.47E-05	3.29E-04	172.3	14.6	20	0.72	13.6	0.25	1.59	100	1.62	0.15	UPb
Lu-2	52.973	6.450	698	Grt (Low Dev)	636	3.53E-05	2.83E-04	175.6	14.6	20	0.39	13.2	0.26	1.8	100	1.60	0.15	UPb
Lu-3	52.979	6.443	502	Grt (Low Dev)	662	4.02E-05	3.00E-04	159.9	17.4	20	0.26	13.5	0.25	1.64	100	1.62	0.19	UPb
Lu-4	52.982	6.439	354	Grt (Low Dev)	887	6.10E-05	3.09E-04	141.1	13.0	20	0.12	13.5	0.25	1.63	100	1.57	0.18	UPb
Lu-5	52.994	6.426	231	Grt (Low Dev)	949	6.71E-05	2.80E-04	138.6	9.6	20	0.24	13.7	0.25	1.56	100	1.63	0.16	UPb
Lu-6	52.967	6.384	126	Grt (Low Dev)	533	3.65E-05	3.51E-04	143.1	12.8	20	0.99	13.6	0.24	1.47	100	1.63	0.16	UPb
Mount Leinster Profile																		
Ml-1	52.618	6.780	795	Grt (Low Dev)	1168	5.94E-05	2.80E-04	191.9	12.2	25	0.48	13.2	0.27	1.46	100	1.63	0.18	UPb
Ml-2	52.618	6.787	596	Grt (Low Dev)	1109	6.56E-05	3.01E-04	184.7	11.4	25	0.21	13.0	0.27	1.45	100	1.64	0.15	UPb
Ml-3	52.611	6.799	421	Grt (Low Dev)	1217	6.60E-05	3.16E-04	180.1	11.2	24	0.68	13.1	0.24	1.27	100	1.62	0.16	UPb
Ml-4	52.599	6.814	159	Grt (Low Dev)	1414	9.12E-05	3.06E-04	172.4	10.4	23	0.17	12.5	0.25	1.27	100	1.65	0.17	UPb
North and West Wales																		
An-1	53.232	4.488	29	Grt (Pre-Camb)	171	8.94E-06	3.78E-04	187.7	29.8	26	0.99	13.2	0.18	1.82	98	1.72	0.18	UPb
Pb-1	51.866	5.282	5	Grt (Ord)	102	4.39E-06	4.43E-04	220.8	52.0	24	0.37	-	-	-	-	1.65	0.20	UPb
Pb-2	51.870	5.283	10	Sdt (Camb)	115	4.85E-06	3.27E-04	230.6	48.0	23	0.76	-	-	-	-	2.10	0.23	UPb
Snowdonia Profile																		
Cu-3	53.187	3.975	869	Grt (Ord)	379	1.33E-05	4.91E-04	280.5	30.0	29	0.53	13.4	0.22	1.35	100	1.72	0.19	UPb
Cu-2	53.191	4.000	701	Grt (Ord)	387	1.49E-05	6.15E-04	252.3	26.0	28	0.66	13.5	0.21	1.4	101	1.79	0.21	UPb
Cu-4	53.209	3.994	327	Grt (Ord)	369	1.43E-05	5.81E-04	250.7	28.0	28	0.61	13.2	0.23	1.4	100	1.70	0.19	UPb
South Wales																		
Brecon Beacons Profile																		
Br-1	51.882	3.708	801	Sdt (Up Dev)	736	3.56E-05	4.87E-04	205.8	16.2	31	0.69	13.9	0.22	1.39	100	1.85	0.27	DA
Br-2	51.853	3.687	505	Sdt (Up Dev)	779	3.62E-05	7.49E-04	213.5	16.6	29	0.87	13.7	0.20	1.27	102	1.73	0.23	DA
Br-3	51.837	3.682	251	Sdt (Up Dev)	838	4.28E-05	7.79E-04	196.9	16.0	38	0.13	13.7	0.21	1.43	100	1.83	0.23	DA
West Britain																		
Isle of Man																		
IoM 1	54.255	4.378	239	Grt (Dev)	800	6.25E-05	5.65E-04	127.6	11.0	20	0.01	12.6	0.28	1.52	101	1.54	0.24	UPb
IoM 2	54.256	4.365	162	Grt (Dev)	765	6.85E-05	6.58E-04	111.2	10.0	21	0.02	13.2	0.24	1.54	103	1.67	0.22	UPb
IoM 3	54.162	4.619	174	Grt (Dev)	376	4.33E-05	9.42E-04	85.5	9.4	20	0.31	13.7	0.21	1.38	100	1.48	0.21	UPb
Southern Upland																		
Sct 1	54.940	3.630	559	Grt (Low Dev)	1303	2.19E-04	5.67E-04	60.4	4.0	20	0.16	13.8	0.17	1.19	103	1.63	0.24	UPb
Sct 2	55.588	4.224	240	Grt (Low Dev)	622	2.02E-05	3.96E-04	299.2	27.6	21	0.27	12.7	0.23	1.43	104	2.03	0.38	UPb
Isle of Arran Profile																		
IoA 1	55.626	5.192	852	Grt (Pal)	49	7.12E-06	3.82E-04	70.6	18.8	18	0.99	-	-	-	-	1.35	0.26	EA
IoA 2	55.626	5.188	746	Grt (Pal)	118	1.79E-05	6.33E-04	61.1	13.4	19	0.11	-	-	-	-	1.37	0.21	EA
IoA 3	55.623	5.177	535	Grt (Pal)	59	1.37E-05	1.76E-04	43.3	15.6	7	0.93	-	-	-	-	1.36	0.15	EA
IoA 4	55.620	5.177	468	Grt (Pal)	106	1.67E-05	3.34E-04	55.3	15.0	15	0.99	-	-	-	-	1.44	0.19	EA
IoA 5	55.617	5.178	385	Grt (Pal)	54	8.04E-06	2.15E-04	59.1	18.8	10	0.97	-	-	-	-	1.38	0.25	EA
IoA 6	55.673	5.206	93	Grt (Pal)	112	1.70E-05	3.40E-04	64.9	16.2	13	0.99	-	-	-	-	1.41	0.23	EA

Sample	U(ppm)	Th(ppm)	Sm(ppm)	Eu (ppm)	Th/U	He (nmol/g)	radius (µm)	masse (µg)	Age (Ma)	± 1σ (Ma)	Ft	Corrected age (Ma)	± 1σ (Ma)
Ire-8													
-a	40.00	149.30	37.30	75.27	3.73	1.73E-05	58.44	6.40	42.4	3.4	0.73	58.0	4.6
-b	38.40	176.68	-	79.92	4.60	1.64E-05	56.87	5.50	37.9	3.0	0.75	50.5	4.0
-c	49.60	162.80	40.32	88.06	3.28	1.89E-05	56.43	5.14	39.5	3.2	0.75	52.5	4.2
-d	57.10	226.32	-	110.28	3.96	2.61E-05	52.40	3.69	43.6	3.5	0.75	58.4	4.7
-e	48.80	153.35	31.50	85.00	3.14	1.84E-05	49.29	3.24	40.0	3.2	0.73	55.1	4.4
Ire-9													
-a	12.80	58.30	21.60	26.61	4.55	8.14E-06	66.79	7.77	56.4	4.5	0.80	70.9	5.7
-d	19.30	77.10	-	37.42	3.99	1.18E-05	64.15	7.80	58.0	4.6	0.75	77.1	6.2
-e	12.70	59.60	20.20	26.81	4.69	7.11E-06	49.67	3.45	48.9	3.9	0.72	67.8	5.4
Ire-10													
-a	30.74	128.14	23.95	60.97	4.17	1.22E-05	43.25	2.84	36.5	2.9	0.65	56.5	4.5
-b	3.83	11.09	-	6.43	2.90	1.36E-07	46.71	2.68	3.9	0.3	0.75	5.2	0.4
-c	4.28	46.70	4.24	15.28	10.91	1.04E-06	45.22	2.73	12.5	1.0	0.71	17.7	1.4
-d	24.92	138.04	34.70	57.53	5.54	7.51E-06	39.97	1.95	23.9	1.9	0.65	36.7	2.9
Bg-1													
-a	44.4	32.9	12.1	52.2	0.74	4.99E-05	79.0	9.67	174.9	14.0	0.847	206.5	16.5
-b	18.2	22.1	6.7	23.4	1.22	1.54E-05	69.7	7.94	118.3	9.5	0.796	148.6	11.9
-d	9.6	11.7	37.8	12.5	1.23	5.61E-06	41.3	2.28	75.4	6.0	0.662	113.8	9.1
-e	14.7	68.2	28.5	30.9	4.63	1.85E-05	47.0	2.87	106.4	8.5	0.725	146.7	11.7
Ga-1													
-a	25.3	86.5	189.5	46.6	3.42	1.87E-05	48.0	1.99	148.9	11.9	0.704	211.5	16.9
-c	20.2	4.6	25.0	21.4	0.23	1.39E-05	43.2	1.90	112.0	9.0	0.681	164.5	13.2
-e	30.6	53.7	-	43.2	1.76	4.95E-05	42.5	1.54	120.7	9.7	0.674	179.1	14.3
Ga-4													
-a	16.2	7.7	-	18.0	0.47	2.45E-05	75.1	9.82	105.5	8.4	0.811	130.1	10.4
-e	3.1	45.1	-	13.7	14.66	4.07E-06	38.5	1.30	54.4	4.4	0.646	84.2	6.7
-c	15.2	0.0	19.9	15.2	0.00	3.40E-06	45.0	1.78	104.3	8.3	0.685	152.3	12.2
Sb-1													
-b	5.3	2.5	-	5.9	0.47	2.29E-06	75.7	9.66	71.7	5.7	0.812	88.3	7.1
-c	4.1	14.1	-	7.4	3.43	2.81E-06	56.2	4.04	64.6	5.2	0.792	81.5	6.5
-e	8.2	2.0	-	8.7	0.25	3.21E-06	42.3	1.76	58.9	4.7	0.674	87.4	7.0
Sb-3													
-a	2.6	35.2	-	10.9	13.39	1.55E-05	68.5	7.42	53.3	4.3	0.792	67.3	5.4
-b	7.0	61.7	-	21.5	8.84	2.45E-05	52.2	4.14	68.9	5.5	0.731	94.3	7.5
-c	9.9	12.6	-	12.9	1.27	3.59E-06	43.0	1.39	52.3	4.2	0.67	78.1	6.2
-d	22.1	38.0	-	31.1	1.72	1.47E-05	55.6	5.09	85.4	6.8	0.75	113.9	9.1
LG 17													
-a	42.20	6.70	-	43.77	0.16	2.62E-05	49.42	3.54	110.1	8.8	0.76	145.0	11.6
-b	30.00	5.50	-	31.29	0.18	1.75E-05	61.24	6.20	102.5	8.2	0.74	137.8	11.0
-e	34.00	34.80	19.30	42.27	1.02	1.76E-05	45.68	2.59	77.0	6.2	0.71	109.0	8.7
LG 18													
-a	23.95	7.30	22.40	25.78	0.30	1.19E-05	53.44	3.96	85.4	6.8	0.77	111.6	8.9
-b	22.60	2.29	27.67	23.28	0.10	9.03E-06	48.27	2.95	71.8	5.7	0.67	107.6	8.6
LG 19													
-a	24.60	1.10	20.60	24.96	0.04	1.26E-05	63.06	6.44	93.1	7.4	0.84	110.5	8.8
-d	39.50	0.80	39.20	39.88	0.02	1.98E-05	55.32	4.36	91.4	7.3	0.77	118.1	9.4
LG 32													
-a	4.50	29.96	14.86	11.62	6.66	4.73E-06	66.61	7.60	75.3	6.0	0.84	89.9	7.2
-b	6.80	50.21	22.60	18.71	7.38	7.61E-06	72.09	9.87	75.1	6.0	0.83	90.1	7.2
-c	20.80	183.21	22.65	63.97	8.81	3.23E-05	86.36	16.54	93.2	7.5	0.84	111.2	8.9
Lu-1													
-a	96.1	1.5	21.6	96.6	0.02	8.69E-05	93.1	18.41	164.6	13.2	0.845	194.8	15.6
-b	24.2	4.7	30.0	25.4	0.20	1.42E-05	56.5	3.93	103.1	8.2	0.777	132.7	10.6
-c	25.6	5.8	31.1	27.2	0.33	1.48E-05	60.9	5.59	98.5	7.9	0.776	126.9	10.2
Lu-3													
-b	21.3	17.1	10.7	25.4	0.80	1.37E-05	66.9	7.16	98.6	7.9	0.812	121.4	9.7
-d	1.9	2.0	5.1	2.3	1.06	4.25E-07	50.7	3.33	33.7	2.7	0.748	45.1	3.6
Lu-4													
-b	4.4	3.5	18.5	5.4	0.80	1.27E-06	54.6	4.06	44.2	3.5	0.766	57.6	4.6
-c	1.0	0.3	3.2	1.1	0.28	2.74E-07	73.2	9.72	47.4	3.8	0.826	57.4	4.6
-d	5.3	24.4	53.6	11.3	4.62	4.22E-06	48.0	1.88	69.8	5.6	0.704	99.2	7.9
Lu-6													
-a	27.7	2.8	23.9	28.5	0.10	8.97E-06	51.3	3.15	58.3	4.7	0.783	74.5	6.0
-b	38.3	0.4	20.2	38.5	0.01	1.40E-05	53.1	3.47	66.0	5.3	0.768	86.0	6.9
-c	36.5	3.1	11.1	37.3	0.08	1.44E-05	63.2	6.29	71.3	5.7	0.797	89.4	7.2
-d	39.6	0.4	25.3	39.9	0.01	1.54E-05	50.3	2.19	71.5	5.7	0.716	99.9	8.0
-e	23.2	0.3	21.4	23.4	0.01	1.31E-05	42.0	1.71	51.9	4.2	0.71	73.1	5.8
Ml1													
-a	52.1	15.9	26.6	55.9	0.30	4.19E-05	57.0	4.63	137.6	11.0	0.775	177.5	14.2
-b	46.4	6.9	22.8	48.2	0.15	3.42E-05	52.8	3.79	130.5	10.4	0.757	172.4	13.8
-c	52.9	45.5	17.6	63.7	0.86	4.53E-05	50.6	3.12	128.9	10.3	0.752	171.5	13.7
Ml3													
-a	49.3	6.9	33.0	51.1	0.14	3.56E-05	64.4	6.48	126.4	10.1	0.803	157.5	12.6
-b	66.7	5.9	25.3	68.2	0.09	5.57E-05	68.3	6.35	149.7	12.0	0.79	189.4	15.2
-e	45.6	8.6	17.4	47.7	0.19	2.68E-05	37.3	1.07	103.4	8.3	0.626	165.2	13.2
Ml4													
-a	72.8	3.0	25.2	73.7	0.04	5.44E-05	60.2	4.86	134.4	10.8	0.799	168.2	13.5
-b	58.6	3.7	26.4	59.6	0.06	4.11E-05	66.2	6.75	126.9	10.2	0.811	156.4	12.5
-c	91.8	4.8	31.3	93.1	0.05	7.26E-05	58.5	4.82	141.8	11.3	0.822	172.5	13.8
-d	91.4	1.0	16.4	91.7	0.01	5.97E-05	39.6	1.38	117.0	9.4	0.705	166.0	13.3
An-1													
-a	5.8	16.7	1.0	9.7	2.88	1.84E-06	38.9	1.59	59.7	4.8	0.65	91.5	7.3
-e	3.9	9.5	2.7	6.2	2.44	1.09E-06	42.9	2.04	45.1	3.6	0.74	61.1	4.9
Pb-1													
-a	2.5	13.4	0.8	5.7	5.36	9.82E-07	35.4	1.20	44.7	3.6	0.65	68.9	5.5
-b	3.4	20.3	15.3	8.2	5.97	1.39E-06	42.9	2.11	55.0	4.4	0.67	81.8	6.5
-e	2.4	25.9	0.0	8.5	10.79	1.25E-06	35.9	1.22	37.5	3.0	0.66	56.9	4.5
Pb-2													
-b	2.1	14.8	41.8	5.8	7.05	7.89E-07	58.4	5.44	43.5	3.5	0.76	57.5	4.6
-d	2.2	7.8	27.6	4.2	3.55	9.69E-07	41.7	2.04	58.2	4.7	0.70	82.8	6.6
Cu-3													
-a	5.5	22.7	62.2	11.1	4.13	3.78E-06	51.4	3.90	85.0	6.8	0.75	112.9	9.0
-b	5.2	23.9	68.2	11.2	4.60	3.56E-06	58.0	5.03	80.3	6.4	0.81	98.8	7.9
Cu-2													
-a	7.3	34.2	53.7	15.6	4.68	3.58E-06	54.3	4.52	70.0	5.6	0.74	94.4	7.5
-c	6.2	42.9	49.5	16.5	6.92	2.47E-06	44.8	2.32	50.9	4.1	0.70	73.0	5.8
-d	6.7	26.3	45.2	13.1	3.93	2.25E-06	37.1	1.45	43.6	3.5	0.66	65.7	5.3
-e	6.0	30.6	55.8	13.5	5.10	1.52E-06	35.5	1.27	34.4	2.8	0.61	56.3	4.5
Cu-4													
-c	3.0	17.0	49.7	7.2	5.67	1.14E-06	42.9	2.11	39.7	3.2	0.72	55.1	4.4
-d	2.8	12.5	50.0	6.0	4.46	1.32E-06	47.2	2.70	56.8	4.5	0.76	74.6	6.0
-e	3.6	15.5	48.3	7.5	4.31	1.74E-06	48.3	2.99	59.3	4.7	0.75	78.7	6.3
Br-1													
-a	3.0	12.9	21.0	6.1	4.28	2.32E-06	53.0	4.13	153.9	12.3	0.69	223.0	17.8
-c	20.1	3.4	28.0	21.0	0.17	1.49E-05	53.0	3.81	178.0	14.2	0.81	220.8	17.7
-d	38.1	3.7	12.1	39.0	0.10	1.58E-05	52.9	3.97	175.3	14.0	0.71	248.6	19.9
-e	3.7	7.6	0.8	5.5	2.05	3.39E-06	59.7	5.65	155.8	12.5	0.80	194.5	15.6
Bn-2													
-e	7.2	12.5	19.0	10.2	1.74	4.68E-06	54.1	4.09	153.7	12.3	0.76	202.4	16.2
Bn-3													
-a	1.2	11.1	1.9	3.8	9.25	1.35E-06	46.0	2.50	89.7	7.2	0.75	119.7	9.6
-b	22.3	6.1	-	23.7	0.27	1.28E-05	40.1	1.82	138.1	11.0	0.70	196.7	15.7
-e	14.6	2.4	3.5	15.2	0.16	9.78E-06	60.4	5.67	158.0	12.6	0.83	190.4	15.2
IoM-1													
-a	1.65	7.93	26.77	3.65	4.81	1.17E-06	50.30	3.27	60.6	4.8	0.77	78.9	6.3
IoM-2													
-c	151.00	8.85	1.23	153.09	0.06	4.80E-05	40.89	1.75	57.9	4.6	0.75	77.0	6.2
-d	55.30	12.04	29.91	58.28	0.22	1.71E-05	43.77	2.20	54.1	4.3	0.75	72.6	5.8
-e	11.80	23.34	6.26	17.32	1.98	5.29E-06	45.24	2.37	56.3	4.5	0.76	74.5	6.0
IoM-3													
-b	16.70	130.52	59.19	47.67	7.82	1.68E-05	61.59	6.16	65.1	5.2	0.83	78.1	6.3
-d	5.00	16.64	45.56	9.14	3.33	2.95E-06	91.66	19.92	60.6	4.9	0.87	69.6	5.6
Sct-1													
-a	38.50	40.72	51.51	48.33	1.06	1.19E-05	49.07	3.64	45.7	3.7	0.72	63.7	5.1
-b	26.40	15.56	23.61	30.18	0.59	7.10E-06	43.58	2.32	43.5	3.5	0.69	62.7	5.0
Sct-2													
-a	3.95	12.37	21.51	6.96	3.13	2.12E-06	54.35	4.45	56.7	4.5	0.76	74.7	6.0
-b	7.10	9.77	8.30	9.44	1.38	2.06E-06	43.47	2.38	40.3	3.2	0.73	55.1	4.4
-c	4.90	11.23	7.12	7.58	2.29	1.71E-06	37.84	1.46	41.6	3.3	0.74	56.4	4.5
IoA-2													
-a	13.70	92.66	197.38	36.46	6.76	6.25E-06	55.47	4.38	32.2	2.6	0.75	42.7	3.4
IoA-4													
-a	7.10	60.93	132.14	22.08	8.58	3.99E-06	45.53	2.42	34.0	2.7	0.70	49.0	3.9
IoA-5													
-c	4.65	14.63	97.72	8.58	3.15	1.98E-06	44.92	2.81	44.4	3.6	0.70	63.2	5.1
IoA-6													
-b	9.30	47.81	164.21	21.36	5.14	5.63E-06	50.29	3.60	49.9	4.0	0.74	67.5	5.4
-d	6.80	30.39	144.05	14.66	4.47	2.89E-06	51.17	3.46	37.7	3.0	0.73	51.7	4.1